Check for updates

Received: 16 July 2021 | Revised: 26 April 2022 | Accepted: 28 April 2022

DOI: 10.1002/esp.5396

RESEARCH ARTICLE

ESPL WILEY

Morpho-sedimentary evolution of a microtidal meandering channel driven by 130 years of natural and anthropogenic modifications of the Venice Lagoon (Italy)

Alvise Finotello[1,2,3] | Ruggero M. Capperucci[4] | Alexander Bartholomä[4] | Andrea D'Alpaos[2,3] | Massimiliano Ghinassi[2]

[1]Department of Environmental Sciences, Informatics and Statistics, Ca' Foscari University of Venice, Venice, Italy

[2]Department of Geosciences, University of Padova, Padova, Italy

[3]Centre for Lagoon Hydrodynamics and Morphodynamics, University of Padova, Padova, Italy

[4]Department of Marine Science, Senckenberg Institute, Wilhelmshaven, Germany

Correspondence
Alvise Finotello, Department of Environmental Sciences, Informatics and Statistics, Ca' Foscari University of Venice, via Torino 155, 30172 Venice, Italy.
Email: alvise.fino@gmail.com

Massimiliano Ghinassi, Department of Geosciences, University of Padova, via G. Gradenigo 6, 5131 Padova, Italy.
Email: massimiliano.ghinassi@unipd.it

Funding information
CORILA; Fondazione Cassa di Risparmio di Padova e Rovigo, Grant/Award Number: HYDROSEM; Università degli Studi di Padova, Grant/Award Number: BIRD168939

Abstract

Tidal channels form the pathways for tidal currents to propagate and distribute clastic sediments and nutrients, thus providing a primary control on tidal-landscape ecomorphodynamics. Most tidal channels in both estuarine and lagoonal environments have a tendency to meander, yet very few studies exist that investigate the full spectrum of processes controlling tidal meander morpho-sedimentary evolution. The Venice Lagoon (Italy) offers a unique opportunity to shed light on this topic, because a long record of morphological and sedimentary data is available, which allows one to relate tidal channel evolution to the hydrodynamic and morphological changes undergone by the lagoon. In particular, during the last 130 years, feedback between rising relative sea levels and anthropogenic interventions has caused severe modifications of the Lagoon hydro- and morphodynamics. Here we investigate how these modifications fed back into the morpho-sedimentary evolution of a meandering tidal channel located in the northern lagoon. Combining extensive datasets of aerial photographs, topographic and bathymetric surveys, geophysical investigations, sedimentary core analysis, and numerical modelling, we show that enhanced local tidal ranges and water discharges determined adjustments of channel cross-sectional geometries proportional to increasing tidal prisms, while changes in local tidal asymmetries caused modifications of the local sediment transport regime, resulting in the development of bar–pool patterns according to the dominant tidal phase. Such bar–pool patterns eventually determined channel migration through a bar-push mechanism controlled by a fluvial-like, quasi-linear relationship between local channel curvature and lateral migration rates. Critical differences in sediment transport regime are, however, highlighted between fluvial and tidal meanders the latter being potentially characterized by high concentrations of suspended sediment during periods of slack waters when wind-driven sediment transport processes are not negligible. This could hamper the formation of high-relief bedforms, with profound implications for the sedimentology of tidal point-bar deposits.

KEYWORDS
bedforms, morphodynamics, numerical modelling, tidal asymmetry, tidal meanders, tidal prism, tidal sedimentology, Venice Lagoon

This is an open access article under the terms of the Creative Commons Attribution License, which permits use, distribution and reproduction in any medium, provided the original work is properly cited.
© 2022 The Authors. *Earth Surface Processes and Landforms* published by John Wiley & Sons Ltd.

1 | INTRODUCTION

Tidal landscapes are commonly dissected by networks of tidal channels that exert a strong control on the ecomorphodynamic evolution of these environments, facilitating the exchange of water, sediments, and nutrients (Coco et al., 2013; D'Alpaos et al., 2005; Hughes, 2012). Tidal-channel evolution, both in time and space, depends on forcings related to both the physical and biological features of the landscapes they wander through (e.g. bank erodibility, sediment characteristics, vegetation cover, bioturbation), as well as to local hydrodynamics, in a fashion that is generally not easily comprehensible because of the relationships and interactions among these forcings and processes (Finotello, Ghinassi, et al., 2020; Kästner et al., 2017; Leuven et al., 2018) acting on overlapping spatial and temporal scales (Feola et al., 2005).

A secondary, yet very important process in tidal network evolution is the meandering behaviour of tidal channels and the resulting point-bar formation (Choi et al., 2004; Choi & Jo, 2015; Dalrymple et al., 2003; Ghinassi et al., 2019; Ghinassi, Brivio, et al., 2018; Hughes, 2012). Besides influencing the planform evolution of the network, meandering impacts the stratigraphy of coastal sedimentary successions, shaping architectures of sedimentary bodies. Indeed, the evolution of tidal meanders is typically recorded in the stratigraphic record through laterally accreted deposits, as well as through channel infilling as the tidal prism (i.e. the volume of water flowing through a given cross-section during half of a tidal cycle; D'Alpaos et al., 2010, 2021) decreases when the channel is partially abandoned via either avulsion or meander cut-off (Brivio et al., 2016; Cosma et al., 2019, 2020; D'Alpaos et al., 2017; Fenies & Faugères, 1998; Ghinassi, D'Alpaos, et al., 2018; Wilson et al., 2017).

Despite their prominence and wide occurrence, however, the characteristics and dynamics of meanders shaped exclusively by tidal flows have frequently been approached assuming a close morpho-sedimentary similarity with their fluvial counterparts (Barwis, 1978; Choi, 2011a; Choi et al., 2004; de Mowbray, 1983), the latter having been studied extensively in the scientific literature (e.g. Hooke, 2013; Ikeda et al., 1981; Lanzoni & Seminara, 2006; Parker et al., 1982; Seminara, 2006). Nevertheless, this assumption is challenged by the observation that several differences exist in the processes that sculpt tidal and fluvial meanders (Finotello, Ghinassi, et al., 2020; McMahon & Davies, 2019), including periodically reversing flows punctuated by slack water intervals, maximum flow discharges not corresponding to bankfull conditions, different external controls on sediment entrainment and deposition (e.g. due to wind-wave action), and a higher spatial density of lateral tributary channels (Finotello, Canestrelli, et al., 2019; Finotello, D'Alpaos, et al., 2020; Marani et al., 2003). Moreover, tidal and fluvial meanders display statistically different morphological properties (Finotello, D'Alpaos, et al., 2020), thus leading to a relevant question, with theoretical and practical implications, that is whether (and to what extent) morphological, dynamical, and sedimentological models derived from the study of fluvial meanders can be extended to their tidal counterparts (Gabet, 1998; Kleinhans et al., 2009; Leuven et al., 2018; Solari et al., 2002). This is especially important in view of the increasing anthropogenic pressures to which tidal coastal landscapes are subjected, thus making it critical to understand how tidal meandering channels respond to natural and anthropogenically induced changes in both external forcings and physical characteristics of the environments they are hosted by.

Here we present multidisciplinary, quantitative analyses aimed to reconstruct 130 years of morpho-sedimentary evolution of a meandering tidal channel located within the microtidal Venice Lagoon (Italy), based on a collection of data derived from both historical and recent aerial photos, tide gauge measurements, bathymetric field surveys, geophysical investigations, and numerical modelling. This work builds upon and complements previous results by Finotello, Canestrelli, et al. (2019), who provided field-based evidence that dominance of tidal flows in tidal meandering channels can be inferred locally from the point-bar patterns, with point-bars developing upstream (downstream) of the meander apex in flood (ebb) dominated settings in accordance with previous experimental findings by Tambroni et al. (2017). In contrast, the present paper aims to unravel how channel cross-sectional geometries and bed morphologies respond to changes in local hydrodynamics, and how such changes ultimately impact meander planform dynamics in terms of channel lateral migration and its relation with local curvature. Moreover, based on novel core-log data, we discuss how alterations in sediment transport regime affected the sedimentology of the studied point bar, as well as the formation of tidal bedforms, which were investigated based on brand new hydro-acoustic data. The ultimate goal of our work is to relate changes in tidal forcings and sediment supply, due to both natural and anthropogenically induced modifications of the lagoon basin, to the morphological evolution, sedimentology, and planform dynamics of the studied tidal meander bends.

2 | GEOMORPHOLOGICAL SETTING AND STUDY AREA

2.1 | The Venice Lagoon

We analysed a high-amplitude meandering reach of the Gaggian channel that wanders through the northern, best naturally preserved part of the Venice Lagoon (Marani et al., 2003) (Figure 1a). The Venice Lagoon, which formed over the last 7500 years covering alluvial Late Pleistocene deposits (Zecchin et al., 2008), is the largest Mediterranean brackish water body, with an area of about 550 km^2. It is connected to the Adriatic Sea through three inlets—namely Lido, Malamocco, and Chioggia from north to south—and is subject to a semidiurnal tidal regime, with an average tidal range of about 1.0 m and peak tidal amplitudes of about 0.75 m around mean sea level (MSL), which can suddenly be increased by meteorological forcings (Carniello et al., 2011; Mel & Lionello, 2014). Seasonal high-tide surges triggered by a combination of astronomical tides and weather conditions cause episodic floodings, locally known as *Acqua Alta* events, in the city centre of Venice and other settlements within the lagoon. These events are typically produced by either strong Sirocco winds blowing from the south-east or Bora windstorms from the northeast (Mel et al., 2019; Rinaldo et al., 2008), and exert pre-eminent control over the medium to long term (i.e. tens to hundreds of years) on the morphodynamic evolution of the lagoon (Carniello et al., 2009). This is especially true for events associated with the Bora wind, which is

the most intense wind in the Gulf of Venice, with velocities that can easily exceed 20 m/s (Figure 1a, inset; see Tommasini et al., 2019).

The tidal regime in the northern Venice Lagoon, where the studied channel is located, has been affected by several anthropogenic interventions over the last centuries (D'Alpaos, 2010; Ferrarin

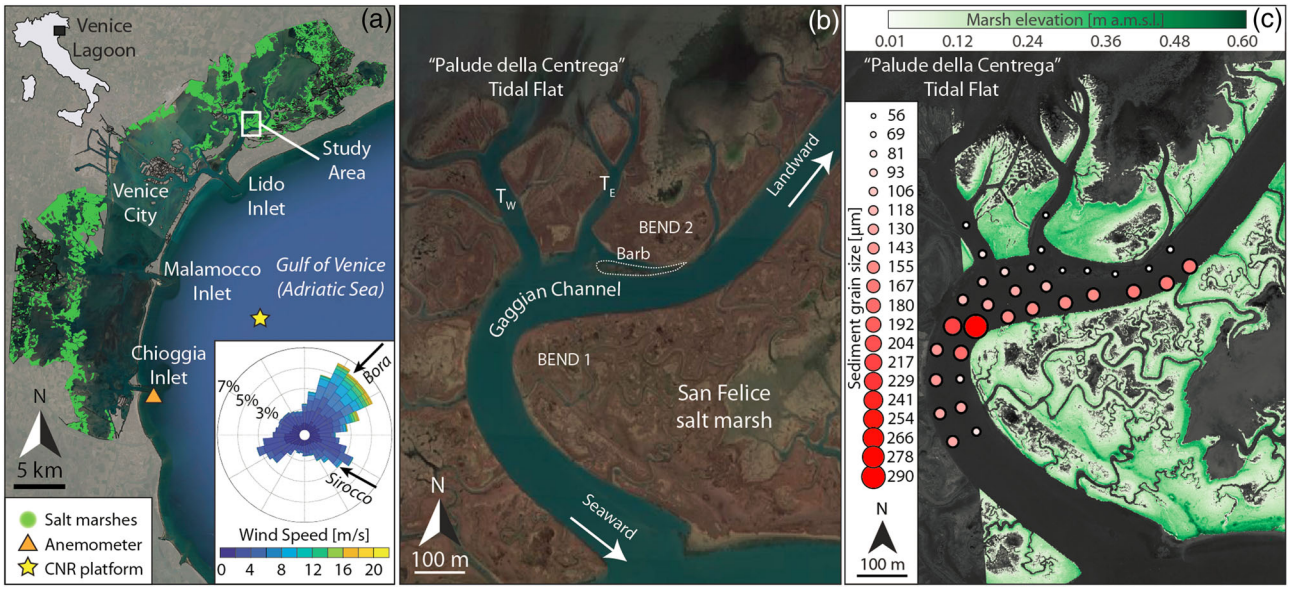

FIGURE 1 Study site. (a) Satellite image of present-day morphology of the Venice Lagoon (Italy). Green areas denote salt marshes. Locations of both the Chioggia anemometric station and of the Consiglio Nazionale delle Ricerche (CNR) Acqua Alta oceanographic platform are also highlighted. Wind-rose diagram representing the wind climate measured at the Chioggia anemometer in 2005 is shown in the lower-right inset (image © Google, Landsat/Copernicus). (b) Satellite image of the study area around the Gaggian channel. All the major morphological features are highlighted, including the two major lateral tributaries (T_E and T_W) connecting the channel to the Palude della Centrega tidal flat to the north (image © Google, Landsat/Copernicus). (c) Salt-marsh elevation in the study area, derived from a flight survey carried out in 2002 (Wang et al., 2009), shown together with sediment grain sizes measured at the bottom of the channel (image © Google, Landsat/Copernicus).

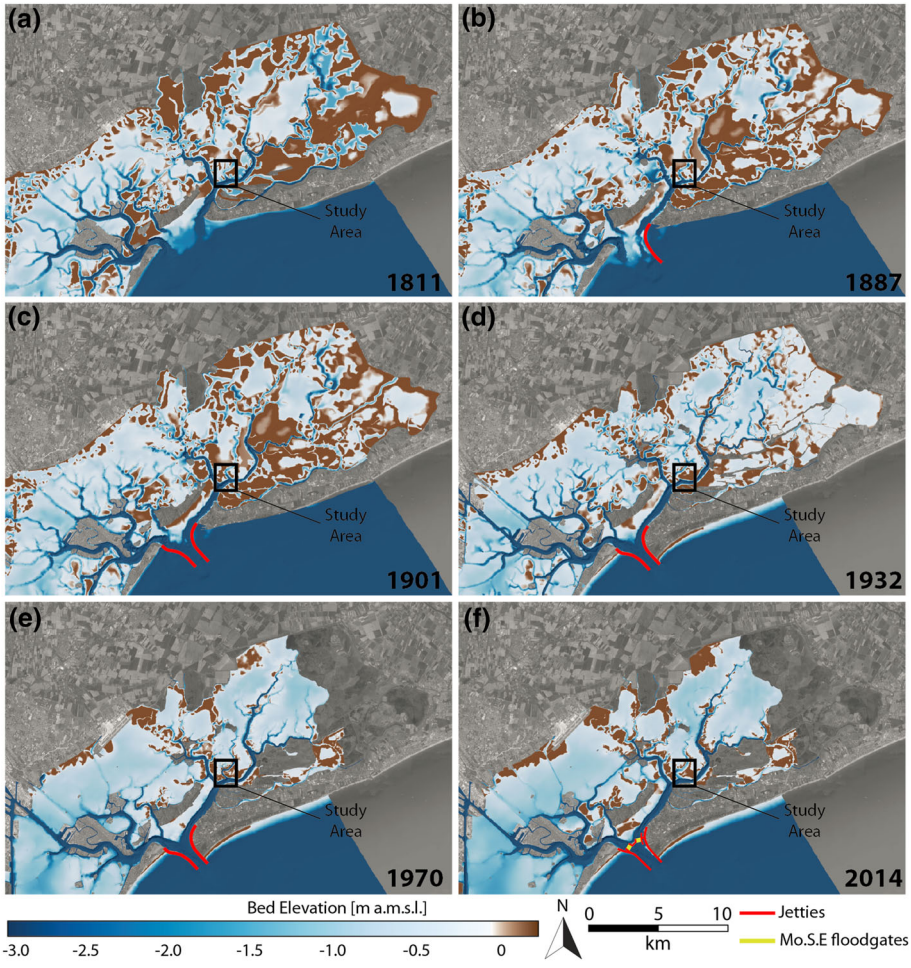

FIGURE 2 Evolution of the northern Venice Lagoon from 1811 to 2014. Colour-coded bathymetries, derived from available topographic data, are over-imposed on a present-day satellite image. Brownish colours approximate salt-marsh extension by denoting areas lying above the mean sea level at the time of the topographic survey. Solid red lines show locations of jetties and seawalls at the Lido inlet, while yellow lines in panel (f) highlight the Mo.S.E. project floodgates. Reduction of the lagoonal area is due to land reclamation.

et al., 2015) (Figure 2). By the end of the 17th century, the Sile and Piave rivers were diverted to the open sea, thus almost entirely eliminating freshwater and sediment inputs. Between 1882 and 1892, massive jetties were constructed at the Lido inlet to allow larger vessels to enter the lagoon. In addition, extensive land reclamation for fish farming and urban development caused a reduction in the total area open to tidal expansion between the 1930s and the 1970s, especially on the edges of the lagoon (Figure 2). Furthermore, prior to 1930, the lagoon was subject to a relative sea level (RSL) rise in the order of 0.15 ± 0.06 cm/year; in the following years, such a rate increased up to 0.38 ± 0.05 cm/year due to the anthropogenically induced subsidence generated by massive groundwater exploitation, which proceeded until the 1970s (Carniello et al., 2009; Ferrarin et al., 2015; Gatto & Carbognin, 1981). The present-day rate of RSL rise is in the order of 0.17 ± 0.04 cm/year (Carbognin et al., 2010; Valle-Levinson et al., 2021). Finally, further modifications to the inlet configuration began in the early 2000s to allow for the installation of mobile floodgates (Mo.S.E. Project) intended to protect the city of Venice and other lagoon settlements from extensive flooding. These modifications caused reductions in tidal amplitude and increases in tidal phase delays within the lagoon (Ghezzo et al., 2010; Matticchio et al., 2017).

The combined effects of these interventions, among which the modification of the inlet morphology is paramount, significantly altered the hydrodynamic regime of the Lagoon. Later studies showed that the average tidal range in the northern Lagoon increased as much as 25% from the construction of the jetties to the 1970s, with local variations being even more pronounced (Ferrarin et al., 2015; Seminara, 2006; Silvestri et al., 2018; Tomasin, 1974). Progressively larger portions of the lagoon became dominated by ebb flows, especially in the areas surrounding the inlets where strong ebb-flow asymmetries enhanced net-sediment export and prevented sediment import from the open sea. As a consequence of sediment loss, both a generalized deepening of tidal flats and a reduction in salt-marsh areas were observed (Carniello et al., 2009; D'Alpaos, 2010; Sarretta et al., 2010).

2.2 | Study area

The study site is a 1300 m-long, 100 m-wide reach of the Gaggian channel comprising two adjacent meander bends, named Bend 1 and Bend 2, which are characterized by average radii of curvature equal to 250 and 200 m, respectively (Figure 1b). Nowadays, the channel is up to 8 m deep and receives tributaries on both its inner and outer banks. Two main tributaries along the outer bank, named hereafter T_W (Western Tributary) and T_E (Eastern Tributary), enter the Gaggian channel near the outer-bank apex of Bend 1 and connect it with the 0.55 m-deep Palude della Centrega tidal flat to the north (Figure 1b). The T_W and T_W tributaries are about 40 and 30 m wide and up to 3.6 and 3.0 m deep, respectively. The present-day channel morphology at Bend 2 is characterized by the presence of an elongated depositional body, similar to a barb in planform, that detaches from the seaward side of the bend (Figure 1b).

The median sediment grain size (d_{50}) at the channel bed is about 129 μm, with cohesive sediment (d < 63 μm) content <20% in volume (Finotello, Canestrelli, et al., 2019). Medium to coarse-grained sand is common in the deepest parts of the channel, whereas fine-grained silty sand occurs in shallower areas and along the thalweg of both T_W and T_E (Figure 1c).

3 | MATERIALS AND METHODS

3.1 | Historical maps and aerial images

A long record of historical topographic maps, high-resolution aerial photographs, and satellite images of the Gaggian channel and its surrounding area is available, ranging from 1901 to nowadays (Figure 3) (Carniello et al., 2009; D'Alpaos, 2010). The 1901 historical map is part of the topographic/hydrographic map of the Venice Lagoon produced by the Genio Civile of Venezia. Aerial photos were retrieved from the 1929–1938 Istituto Geografico Militare (IGM) flight survey (1938), the IGM 1955 Gruppo Aereo Italiano flight survey (1955), the Compagnia Generale Riprese aeree Parma, Veneto Region aerial photo survey (1968), the Regione del Veneto – L.R. n. 28/76 Formazione della Carta Tecnica Regionale aerial photogrammetric survey (1978, 1987, 1995). All images are freely available from the Atlante della Laguna (http://www.atlantedellalaguna.it/) and/or—upon registration—from the Circe Laboratory of Cartography and GIS of the IUAV University of Venice (https://circe.iuav.it/catalogo-foto-aeree/). Satellite images (2001, 2014) are Landsat/Copernicus products that were accessed through Google Earth™. All available images were georeferenced with ArcGIS 10 (Esri) and then overlaid to quantify channel lateral migration. The latter was computed based on changes in the position of the channel centreline, derived from manual digitalization of channel banks for all the available aerial images, and measured at a spatial resolution of 2 m (see Figure 3). We utilized a standard dynamic time warping (DTW) algorithm implemented in R (Giorgino, 2009) and performed through the QGIS software (v.3.6.3) processing tool. The DTW algorithm represents the state-of-the-art method to compute lateral channel migration in dynamic meandering systems. It employs a cost matrix to minimize the sum of distances between two consecutive channel centrelines, weighted by both the spatial distance and the similarity in local channel curvature. In doing so, it monitors changes in channel centreline location and curvature (see Sylvester et al., 2019 for further details; Donovan et al., 2021; Finotello, D'Alpaos, et al., 2019; Ielpi et al., 2020). In more detail, DTW alignment of the initial and final channel centrelines is performed using a Euclidean distance matrix for corresponding spline points, augmented with the third dimension of curvature at those points. That is, for each point i of the original centreline and j of the final centreline, the following matrix of distances is computed:

$$d_{i,j} = \sqrt{\Delta^2{}_{i,j} + \lambda^2 \left(C_i - C_j\right)^2}$$

where $\Delta_{i,j}$ denotes the Euclidean (i.e. planar) distance between i and j, C is the local channel-axis curvature, and λ is a multiplier parameter used for weighting curvature values. Given the limited migration rates that characterize our studied channel (see Section 4), we adopted a reduced value of $\lambda = 10^3$ m^2, thus giving more emphasis to centreline spatial proximity.

Besides computing migration rates, comparison among the different available photos also allowed us to outline changes in the width of the main channel and its tributaries, as well as to identify the establishment of depositional or erosional processes along specific portions of the channel banks.

3.2 | Bathymetric and topographic data

Elevation data, both within the Gaggian channel and along the salt marshes flanking it, are available since 1901 from the topographic/hydrographic map of the Venice Lagoon produced by the Genio Civile of Venezia. Elevation data for the 1932 and 1970 configurations were also obtained from the bathymetric maps of the Venice Lagoon produced by the Venice Water Authority (Magistrato alle Acque). The elevation data were georeferenced and analysed in a GIS environment (ArcGIS 10, Esri), spatially interpolating the data points through a cubic spline method with a grid spacing varying between 0.8 and 3 m, according to the spatial density of the original data (Figure 4). Additionally, two geophysical surveys were carried out in 2011 and 2020 to provide bathymetries and a detailed image of the possible channel seabed structures (e.g. bedforms), which were not previously described in the literature (Finotello, Canestrelli, et al., 2019; Ghinassi, Brivio, et al., 2018; Madricardo et al., 2017). In 2011, geophysical data were acquired by means of an Innomar SES 2000 compact parametric sub-bottom profiler. Overall, 27 profiles were collected: 2 longitudinal and 22 cross-sectional profiles along the Gaggian channel, and 3 along-channel profiles within the T_E and T_W tributaries (Figure 4d). Position data were recorded via GPS [two TOPCON GR-3 receivers—dual frequency (L1/L2) and dual constellation (NavStar/Glonass), with integrated UHF Tx/Rx radios were used] and processed using Geo Office software (Leica).

A second survey was carried out in summer 2020 using an Innomar SES 2000 standard plus (parametric sub-bottom profiler) and a Starfish 452f sidescan sonar. The SES was pole-mounted at the bow of a 6 m aluminium catamaran in order to minimize the noise due to

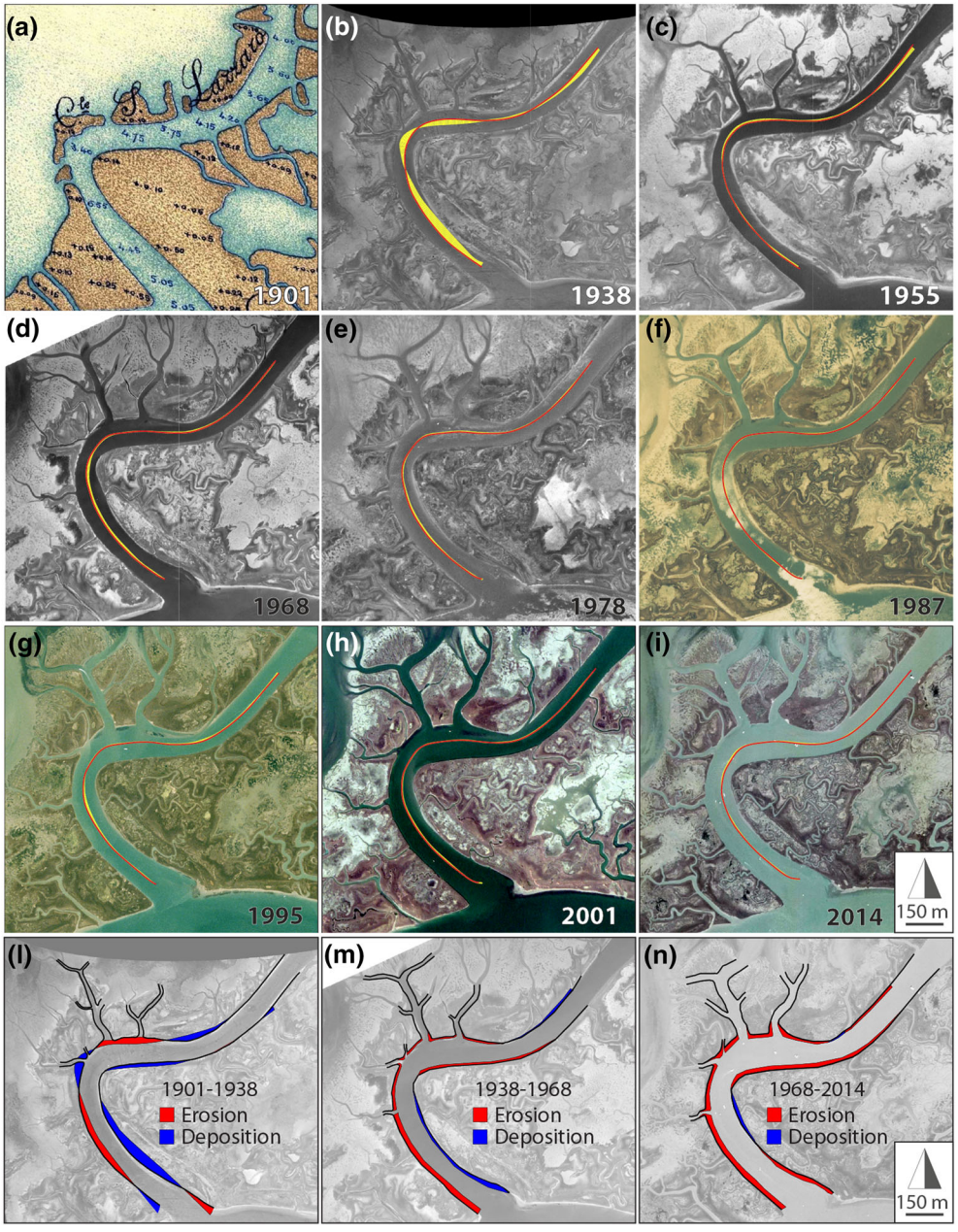

FIGURE 3 Planform evolution of the study channel. (a–i) Historical maps and aerial images showing the evolution of the study area between 1901 and 2014. In each panel, red lines denote the position of the channel centreline, whereas yellow lines represent migration vectors, relative to the previous channel configuration, computed through a dynamic time warping algorithm. Erosional and depositional patterns reconstructed from the available images are also shown for the periods 1901–1938 (l), 1938–1968 (m), and 1968–2014 (n), approximately corresponding to the time intervals investigated through numerical simulations.

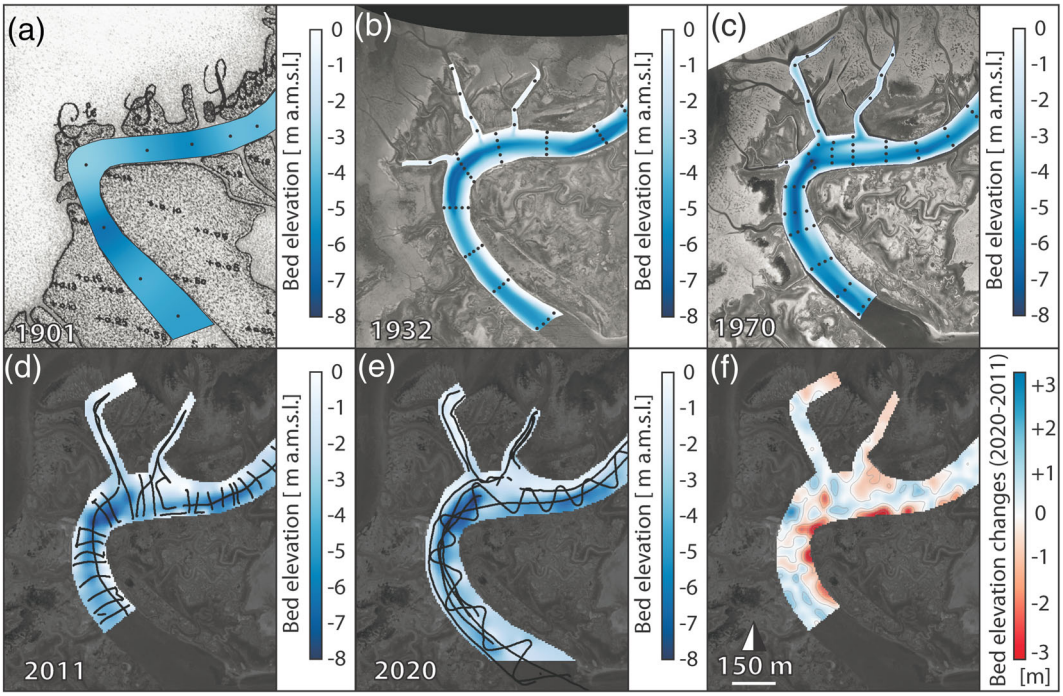

FIGURE 4 Depth evolution of the Gaggian channel. (a) 1901 bathymetry derived from the Genio Civile di Venezia topographic/hydrographic map of the Venice Lagoon; black dots show the position of available data points used for spatial interpolation. (b, c) 1932 and 1970 bathymetries based on the bathymetric map of the Venice Lagoon by the Magistrato alle Acque (Venice water authority); black dots show the position of available data points used for spatial interpolation. (d) Bathymetry obtained from the 2011 geophysical data. Tracks of the sub-bottom profiler are highlighted by black solid lines. (e) Bathymetry calculated from the 2020 geophysical data. Tracks of the sub-bottom profiler are highlighted by black solid lines. (f) Bathymetric changes observed in the study area between 2011 and 2020, based on data reported in panels (d) and (e).

the boat engine, and the sidescan sonar was side-mounted on the starboard of the boat. The positioning was recorded by means of a Trimble SPS852 rover/base system, including RTK corrections for high accuracy. Four longitudinal profiles covered the Gaggian channel parallel to its borders. A zig-zag profile crossed the channel over the entire length of the study area (Figure 4e). The Innomar ISE software was employed for extracting the channel depth from the sub-bottom high frequency (100 kHz) and the resulting {*x*, *y*, *z*} data were gridded by means of Surfer 13 (Golden Software) using the Kriging algorithm. The sidescan sonar data were exported in xtf. format and processed with SonarWiz 7.2 software. Geometric and radiometric corrections were performed, as well as slant range and offset corrections. All data were eventually analysed using GIS software (ArcGIS 10, Esri).

The different datasets were employed to monitor changes in bed morphologies, cross-sectional geometries, and channel bedforms, when possible. Besides, bathymetric data were used to assign bed elevation to the computational grids employed for numerical modelling (see Section 3.4).

3.3 | Sedimentological data

Sedimentary cores were recovered along the seaward side of the point-bar associated with Bend 1 (Figure 1b) from deposits accreted between 1901 and today. Two cores were recovered from a depth of 2 m using a vibrocorer, equipped with an aluminium liner (8 cm in diameter). An additional core was collected from a depth of 4.5 m using an Ejikelkamp hand auger, through a gouge sampler with a length of 1 m and a diameter of 30 mm. All the recovered cores were cut longitudinally, photographed, and logged. Core logging included a macroscopic description of sediment grain size, sedimentary structures, vertical grain-size trends, degree of bioturbation, and occurrence of plant and/or shell remains. The core halves' surface was glued using wood stain and peeled in order to create a storable record of the cores and to highlight sedimentary structures.

3.4 | Numerical modelling

In order to analyse temporal changes in flow and sediment-transport regimes along the studied bends, we carried out several numerical simulations using the finite-element, bidimensional (depth-averaged), hydrodynamic and wind-wave model developed by Carniello et al. (2011). The model—which is suitable to reproduce tidal flows, wind waves, and the related sediment transport processes in shallow microtidal basins—has been widely tested and calibrated against modern and historical field data from the Venice Lagoon (Carniello et al., 2005, 2009, 2011, 2012; Tommasini et al., 2019). While a brief introduction to the modelling approach is provided in the following paragraphs, the reader is referred to Carniello et al. (2005, 2011, 2012, 2014) for extensive descriptions and details concerning the calibration of model parameters and their match to field measurements and remote-sensing data in terms of water levels, wave heights, flow rates, and suspended sediment concentrations.

The model consists of a hydrodynamic module that solves the depth-averaged shallow-water equations, suitably modified to reproduce wetting and drying processes in very shallow and irregular domains, using a semi-implicit staggered finite element method based

on the discontinuous Galerkin approach (after Defina, 2000). The hydrodynamic module is coupled with a wind-wave module that reproduces the generation and propagation of wind waves in shallow-water tidal environments, solving the wave-action conservation equation parameterized using the zero-order moment of the wave action spectrum in the frequency domain (Carniello et al., 2005, 2011). Outputs from the hydrodynamic and the wind-wave modules are finally employed by a sediment-transport and bed-evolution module, which solves the advection–diffusion equation and the related processes of sediment entrainment, transport, and deposition that control bed evolution (Carniello et al., 2012). Notably, the model accounts for the simultaneous presence of both cohesive (i.e. muddy) and non-cohesive (i.e. sandy) sediments, as well as for the nonlinear interactions between bottom shear stresses induced by wind-wave (τ_{ww}) and tidal currents (τ_b) in determining the total bottom shear stress (Soulsby, 1997).

Several accurately calibrated WWTM computational grids reproducing the whole Venice lagoon in its past and present configurations already existed and had been used in previous studies (Carniello et al., 2009; Finotello, Marani, et al., 2020; Silvestri et al., 2018; Tommasini et al., 2019). Here we considered the grids representing the lagoon morphology in 1887, 1901, 1931, 1970, and 2014. The available grids account for: (i) the construction of the jetties at the Lido inlet, completed between 1882 and 1892; (ii) the progressive deepening of the lagoon; and (iii) the loss of salt marshes and lagoonal areas due to both natural processes and land reclamation (Figure 2). The spatial resolution of the computational grids has been refined in the study area, in order to provide more detailed results along the studied channel. The bathymetries of the computational grids were reconstructed from the available elevation data, and are referred to the MSL recorded when each survey was performed. In this way, RSL rise was implicitly accounted for since all the numerical simulations were performed by forcing the model with tidal waves imposed at the open sea boundary and oscillating around the MSL (Carniello et al., 2009; Silvestri et al., 2018).

Two distinct series of numerical simulations were carried out. For both series, boundary conditions are the same as those employed by Finotello, Canestrelli, et al. (2019), but additional simulations were carried out, including the 1901 and 1887 configurations of the lagoon, in order to better highlight changes in tidal propagation and wind-wave-induced sediment transport processes across the tidal basin, and their effects on the studied meander morphodynamics. First, we simulated the propagation of a semidiurnal (M_2) tide characterized by an amplitude of 0.5 m akin to typical spring tides in the High Adriatic Sea (D'Alpaos, 2010; Townend, 2010). These simulations were aimed at providing an overview of the changes in local hydrodynamics and the related sediment-transport processes that occurred along the Gaggian channel over the last 130 years. Therefore, no wind-wave-related processes were considered. Second, variations in the sediment transport regime associated with both wind waves and tidal currents were investigated by simulating 28 days of tides and wind waves. We took advantage of hourly tidal levels and both wind velocities and directions measured, respectively, at the Acqua Alta oceanographic platform and the Chioggia anemometric station (Figure 1a) from 16 November to 14 December 2005. This time span embodies a probability distribution of wind velocities and directions that makes it representative of the typical wind field observed within the Venice Lagoon over much longer periods of time (D'Alpaos et al., 2013). In particular, the 28-day period selected for our simulations is characterized by strong Bora windstorm events with velocities exceeding 20 m/s (see details in Finotello, Canestrelli, et al., 2019, their Figure 6), thus allowing us to focus on the role of storm-induced sediment resuspension on the sediment transport regime in the study area.

4 | RESULTS

4.1 | Morphological evolution

During the last 130 years, only minor changes were observed in the overall planform morphology of the studied channel (Figure 3). Nonetheless, analyses of aerial images show that the average channel widths (± standard deviation) increased by 38%, from 81.96 ± 14.04 m in 1901 to 113.53 ± 23.47 m in 2014. The most pronounced widening occurred between 1932 and 1955, when the channel increased its width at a rate of about 0.63 ± 0.22 m/year, compared to a width increase of 0.11 ± 0.06 and 0.46 ± 0.11 m/year in the periods 1901–1932 and 1968–2014, respectively. Dynamic time warping analysis of channel centreline migration (Figure 3) (Donovan et al., 2021; Finotello, D'Alpaos, et al., 2019; Ielpi et al., 2020; Sylvester et al., 2019) indicates an average migration rate equal to 0.38 ± 0.36 m/year throughout the whole study period, corresponding to a normalized migration rate of about 0.4% of channel width per year, with a peak value of 0.51 ± 0.54 m/year observed between 1987 and 1995. A clear change in the type of meander planform evolution, from symmetric expansional to downstream translational, is observed between 1901 and 1938. From 1938 onwards, centreline migration appears more pronounced on the seaward side of bend apexes, especially for Bend 1, whereas the migration trajectory of Bend 2 is less obvious, likely because of disturbance imposed by complex bank evolution dynamics at the outflow of both the T_E and T_W tributaries, where significant widening is observed throughout the years (Figure 3). The magnitude of migration seems to decrease progressively through time, with the lowest migration rates among all the analysed time intervals recorded for the period 2001–2014, when the direction of migration appears to be reversed compared to previous trends. Specifically, the channel centreline moved preferentially towards the inner (convex) bank in the area around the apex of Bend 1, thus giving rise to inner bank erosion that is also reflected by the bathymetric changes between 2011 and 2020 (Figure 4f).

The bathymetry of the Gaggian channel underwent significant modifications during the last century, with a progressive deepening that occurred mostly between 1932 and 1970 (Figure 4). Such a deepening trend is also observed in the surrounding area, where the Palude della Centrega tidal flat (Figure 1b) steadily deepened from 0 to −0.63 m below MSL between 1901 and 1970, before slowly recovering elevation up to −0.55 m in 2014 (Ghinassi, Brivio, et al., 2018). Clearly, caution should be employed when interpreting the results derived from the 1901 bathymetry which, although derived using state-of-the-art topographic techniques, suffers from a lack of data points within the studied channel (Figure 4a). In spite of this, however, the distribution of channel depths observed from the available data exhibits reduced depth at the bend apex and maximum depth at the

bend inflection points, a result that is consistent with the nearly symmetric local tidal regime that characterized the studied channel when the bathymetric survey was carried out (see Section 4.2; see also Finotello, Canestrelli, et al., 2019 for a detailed discussion). In terms of meander-bend morphologies, the 1901 historical map suggests that both Bend 1 and Bend 2 were characterized by two pool areas located immediately landward and seaward of the bend apexes (Figure 4a). From 1932 to nowadays, the pool areas became progressively deeper and moved towards the bend-apex zone, being regularly interspaced by shallower riffle zones at the meander inflection points (Figures 4b-e). During the same period, the barb grew on the seaward side of Bend 1: it became wider and shallower through time, and its topset is nowadays characterized by elevations in the range 0.4–0.8 m below MSL, being almost exposed at low tides. Comparison between the 2011 and 2020 bathymetries (Figure 4f) highlights rapid changes of the channel bed morphology over a relatively short time span, especially in the area facing the T_W and T_E outlets. However, the resulting differential bathymetry appears quite noisy, such that no clear trends emerge in the morphological evolution of the channel aside from a relatively widespread erosion occurring along the inner bank of Bend 1. Such unexpected erosion at the meander inner bank, together with the high level of noise observed from the data, might be related to the significant anthropogenic modifications of the Lido inlet morphology that were put in place between 2006 and 2014 to accommodate the Mo.S.E. floodgates. These modifications significantly altered the hydrodynamic regime of the lagoon (see details in Section 5.1), especially in tidal channels located relatively close to the inlets such as, for example, the Gaggian channel (Matticchio et al., 2017), in this way producing non-negligible morphological adjustments. Further detailed morphological studies would, however, be required in order to better elucidate this hypothesis.

In spite of all these morphological changes, all the relevant meander morphometric features exhibited by Bend 1 and Bend 2—including wavelength, curvature radius, bankfull depth, and bend amplitude—consistently scaled to the average meander width and remained within the range of variability typically observed for tidal (as well as fluvial) meanders (Figure 5).

4.2 | Hydrodynamics and sediment transport regime

Numerical simulations suggest that profound changes in local hydrodynamics occurred from 1887 to today. In particular, damping of the tidal wave was progressively reduced, such that the local tidal range increased continuously from 0.36 m in 1887 to 0.74 m in 2014, rising 67% (from 0.36 to 0.60 m) in the period 1887–1901 alone (Figure 6b). Changes in the local tidal range were accompanied by rises of both flow velocities (v) and discharges (Q_w) through the Gaggian channel (Figures 6a and c). Two major incremental steps are observed during the study period, especially in terms of v, which occurred from 1887 to 1901 and from 1932 to 1970, respectively (Figure 6a). The reader is referred to Finotello, Canestrelli, et al. (2019) for details about distribution and changes through time of depth-averaged and three-dimensional (i.e. cross-sectional) velocities within the studied channel. Variations of the maximum ebb and flood velocities through time also determined changes in the local peak flow asymmetry (ρ_s). The latter parameter is defined as the ratio between the flood and the ebb maxima of cross-sectionally averaged velocities (Friedrichs & Aubrey, 1988), and is suitable to discriminate flood-dominated ($\rho_s > 1$) and ebb-dominated ($\rho_s < 1$) flows within tidal channels (Finotello, Canestrelli, et al., 2019; Guo et al., 2019). In the Gaggian channel, ρ_s reduced from 1.07 in 1887 to 1.01 and 0.88 in 1901 and 1932,

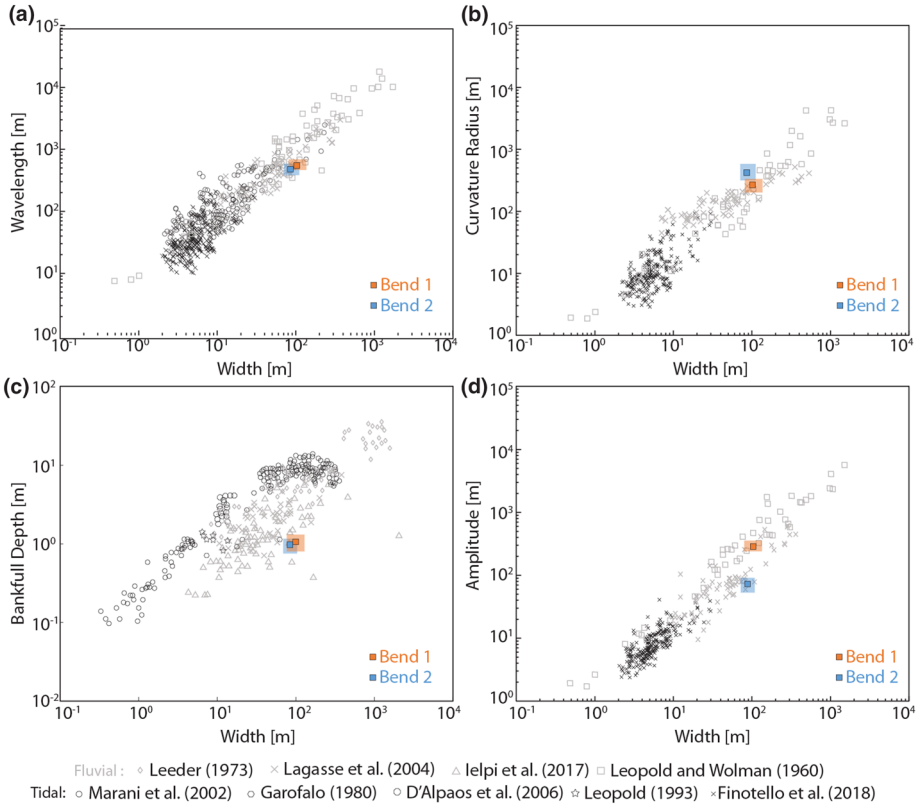

FIGURE 5 Planform features of the Gaggian channel's Bend 1 and Bend 2 compared against literature data on both tidal and fluvial meanders (see Finotello, Ghinassi, et al., 2020 and references cited therein). Average meander width is plotted against (a) meander wavelength, (b) meander radius of curvature, (c) meander bankfull depth, and (d) meander amplitude. Squares represent data for the Gaggian channel derived from aerial images and averaged over the entire study period (Figure 3), whereas the shadowed areas denote the associated range of variations.

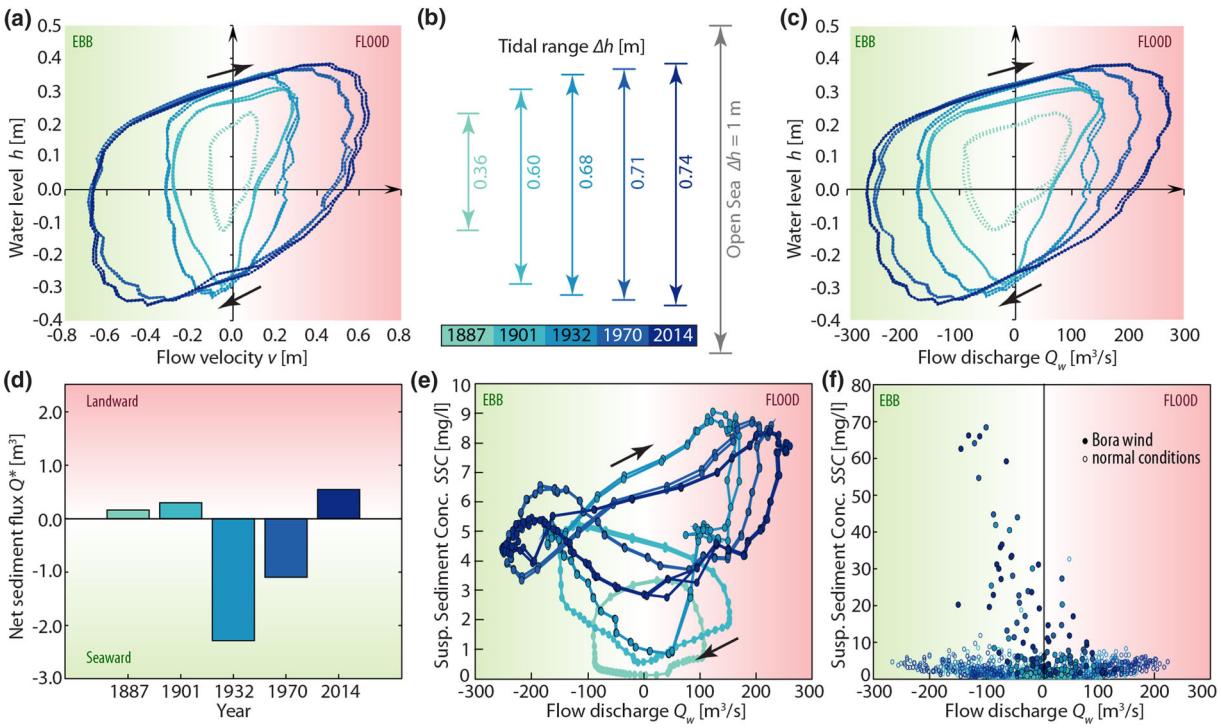

FIGURE 6 Results of numerical simulations. (a) Variations in water levels *h* and associated average flow velocities *v* within the Gaggian channel over two complete semidiurnal tidal cycles. (b) Changes in the Gaggian channel's local tidal range through time. (c) Variations in water levels *h* and associated average flow discharges Q_w within the Gaggian channel over two complete semidiurnal tidal cycles. (d) Net sediment flux Q^* through the Gaggian channel over a complete semidiurnal tidal cycle. (e, f) Variations in suspended sediment concentration SSC and associated average flow discharges Q_w within the Gaggian channel over two complete semidiurnal tidal cycles. All the results were obtained imposing a 0.5 m-amplitude semidiurnal (M_2) tide at the open sea boundary, except for panel (f) that refers to a 28-day-long simulation carried out using hourly measured tide and wind data (see Section 3.4). Filled dots in panel (f) denote SSC associated with Bora windstorm events, whereas empty dots refer to normal, windless conditions. Colours in each panel denote different years according to the colour bar shown in panel (b).

respectively. After that, it remained nearly constant in 1970 ($\rho_s = 0.89$) before increasing to 1.04 in 2014.

Analyses of numerically simulated sediment transport processes highlight changes in the direction of net sediment transport (Q^*) over a single tidal cycle according to changes in ρ_s (Figure 6d) (Finotello, Canestrelli, et al., 2019). The suspended sediment concentration (SSC) in the absence of wind is strongly correlated with flow discharges and never exceeds 10 mg/L, with values below 5 mg/L between 1887 and 1901 (Figure 6e). Notably, SSC does not fall to zero even when tidal flows are absent (i.e. slack-water periods corresponding to $Q_w = 0\ m^3/s$), and SSC associated with ebb slacks is typically larger than those observed during flood slacks (Figure 6e). Numerical simulations carried out with observed tidal and wind data suggest that in 1887 and 1901, Bora windstorm events had limited influence on SSC, the latter always being lower than 10 mg/L (Figure 6f). In contrast, starting from 1932, SSC reaches maximum values up to 70 mg/L during Bora windstorm events and easily exceeds 10 mg/L even during slack waters (Figure 6f).

4.3 | Bedforms

The 2020 sidescan data highlighted the presence of channel bedforms, in the form of dunes, within a restricted area immediately downstream of the Bend 1 apex (Figure 7a). These dunes are characterized by lengths (*L*) ranging between 2.80 and 18.88 m (mean value 5.66 ± 2.59 m) and heights (*H*) varying from 0.01 to 0.34 m (mean value 0.10 ± 0.06 m). They also appear to be nearly symmetric on average, since their mean asymmetry index is $\overline{\mathcal{A}_i} = 0.01 \pm 0.29$, $\mathcal{A}_i$ being defined as $\mathcal{A}_i = (\ell_u - \ell_d)/L$, where ℓ_u and ℓ_d denote the distance between the dune crest and its upstream and downstream troughs, respectively. Estimates of average flow depths (*h*) above the dunes were also obtained from numerical simulations, which provided values within the range 4.3–6.3 m (mean value 5.10 ± 0.52 m). Values of the dune lee-side angles were also derived from the available SES data. The average maximum and mean lee-side angle, computed following the approach proposed by Cisneros et al. (2020), is equal to 2.51 ± 1.67° and 2.09 ± 1.51°, respectively, whereas the highest lee-side angle observed in the Gaggian channel is equal to 9.69° (Figure 7).

4.4 | Point-bar deposits

Point-bar deposits are located on the seaward side of Bend 1 and are 4.5–5.5 m thick. Analyses of seismic images (see Ghinassi, Brivio, et al., 2018) show that beds consistently dip c. 10–20° towards the channel thalweg without relevant truncations, but these beds are locally truncated by the present-day inner bank of the channel. Point-bar deposits cover a layer of medium sand with fragmented shells and pebble-size mudclasts. That layer represents older thalweg deposits. Point-bar deposits show an overall fining-upward grain-size trend from medium to fine sand with mud to mud, with millimetric laminae of fine to very fine sand (Figure 8). Sandy bar deposits include

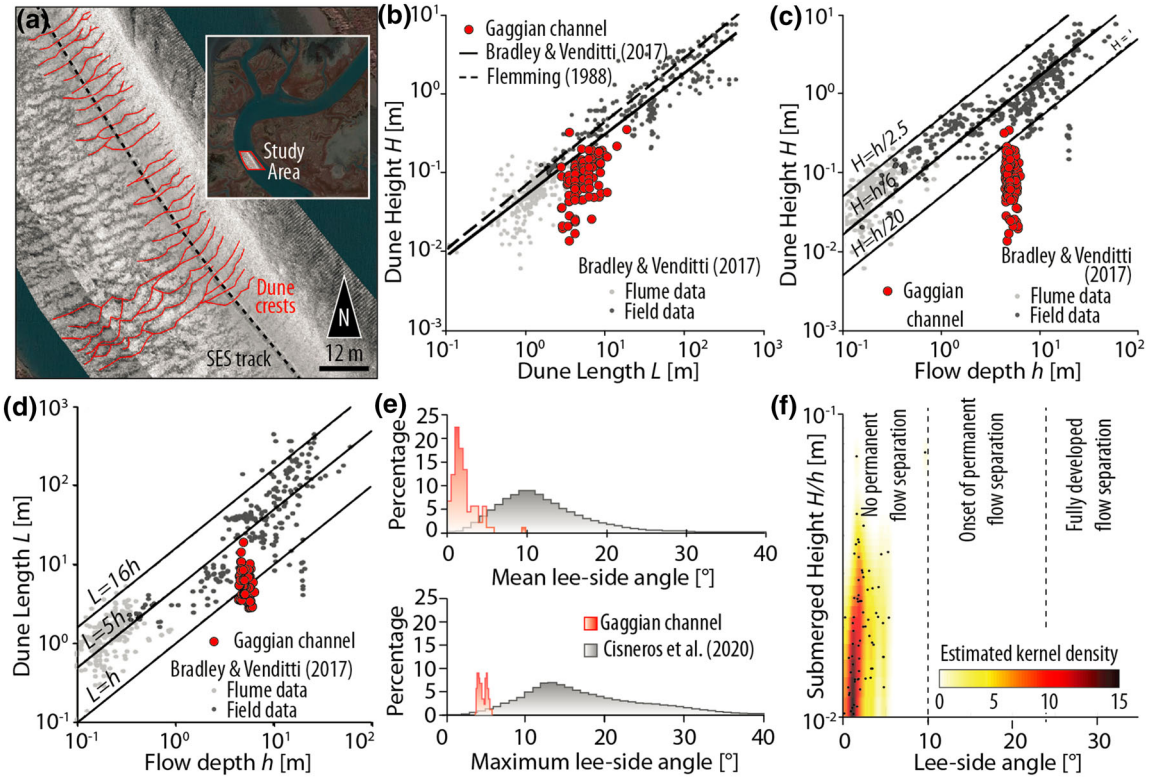

FIGURE 7 Channel bedforms. (a) Location of the bedforms and detailed view of the sidescan data. Black dashed line represents the SES track, which was used for extracting the bathymetric data, whereas red lines denote hand-digitized dune crests. (b) Dune height (*H*) plotted against dune length (*L*). Red dots represent data from the Gaggian channel. Field and flume data derived from data compilation by Bradley & Venditti (2017), together with best-fit power law by both Bradley & Venditti (2017) and Flemming (1988), are also reported. (c) Dune height (*H*) plotted against flow depth (*h*). Red dots represent data from the Gaggian channel. Field and flume data derived from data compilation by Bradley & Venditti (2017), together with lines representing different *H*/*h* ratios, are also reported. (d) Dune length (*L*) plotted against flow depth (*h*). Red dots represent data from the Gaggian channel. Field and flume data derived from data compilation by Bradley & Venditti (2017), together with lines representing different *L*/*h* ratios, are also reported. (e) PDF plots for the mean and maximum dune lee-side angles measured in the Gaggian channel. Data from fluvial dunes compiled by Cisneros et al. (2020) are also reported for direct comparison. (f) Hotspot graph of the potential for flow separation in which the submerged dune height (*H*/*h*) is plotted against the dune lee-side angle. Limits of the zones of no-flow separation, the onset of flow separation, and fully developed zone separation according to Lefebvre & Winter (2016) are also reported.

scattered shell fragments, and muddy layers are enriched in comminuted plant debris. Both sandy and muddy bar deposits are characterized by a pervasive lamination dipping towards the channel thalweg, consistent with the overall bar bedding. The dip angle of the laminae is c. 10–20°, and evidence of cross-stratifications is almost missing. The very few lamina set are up to 1 cm thick. Laminations are defined by the alternation of sand and mud, which range in thickness between 0.3 and 30 mm. Only in the lowermost part of the bar, sandy layers can be up to 5–15 cm thick. Laminae do not show any clear cyclic change in thickness, except for localized thinning or thickening-upward trends developed at millimetric scale. Couplets of 0.3–0.5 mm muddy laminae, which embed a 0.5–1 mm drape of sand, are common in the middle to upper part of the bar. The upper part of the bar mud is pervasively oxidized and has root remains associated with the development of halophytic vegetation.

5 | DISCUSSION

5.1 | Morphodynamics

Morphological features of the study-case meander bends are consistent with those observed for other tidal and fluvial meanders worldwide (Finotello, D'Alpaos, et al., 2020) (Figure 5), suggesting that results obtained in this area could be extended beyond the specific study site at hand, at least in terms of planform morphologies and dynamics. The observed bank-migration rates (mean value $\overline{M_R} = 0.38 \pm 0.36$ m/year) are consistent with values typically observed in tidal meanders within the Venice Lagoon (Finotello et al., 2018; McClennen & Housley, 2006) and other tidal systems worldwide (Gabet, 1998; Garofalo, 1980). More importantly, M_R does not appear to be correlated with either the observed changes in channel width (ΔB) or rates thereof (ΔB_R) (Figures 9a and b). This would exclude the chance that the observed bank migrations were simply due to channel widening driven by increased tidal prisms (D'Alpaos et al., 2010), rather than to actual meander dynamics. Indeed, time-lapse analyses of bank migration suggest that width-adjusted migration rates ($M_R^* = M_R \cdot B$ [−]) are strongly controlled by dimensionless channel curvature ($C^* = C \cdot B$ [−]) in a fluvial-like fashion (Hickin & Nanson, 1975; Hooke, 2013). Particularly, we show that both median and 95th values of the M_R^* distribution, corrected by the spatial lag between maxima in migration rate and curvature (Sylvester et al., 2019), exhibit a linear functional relationship to C^* for C^* values <0.25, and then plateau at $C^* > 0.25$–0.50 (Figure 9c). This corroborates previous results (Finotello et al., 2018) suggesting that tidal meanders recapitulate fluvial-meander morphodynamics by essentially

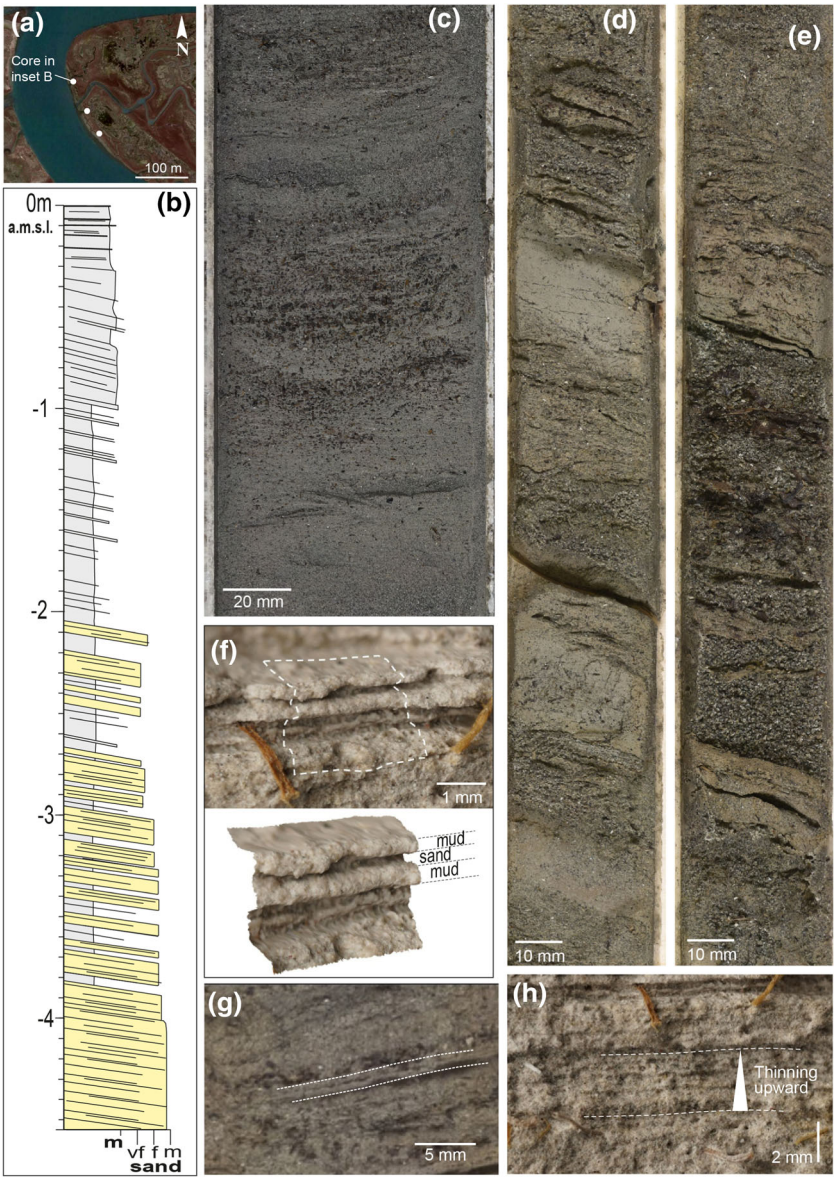

FIGURE 8 Sedimentary features of point-bar deposits at Bend 1. (a) Location of recovered sedimentary cores. (b) Vertical grain-size distribution in core 2. (c–e) Lamination in point-bar deposits. Note that laminae are commonly marked by plant debris, and that no changes in dip angle occur within single cores. (f, g) Couplets of muddy laminae embedding a drape of fine sand. (h) Subtle upward thinning of laminae.

replicating the same physical mechanisms driving meander planform dynamics. The paramount control exerted by channel curvature on tidal meander evolution is further supported by the analyses of bank migration in relation to other hydraulic parameters, such as tidal asymmetry (ρ_s) and tidal prism (P), which we computed taking advantage of outputs from our numerical simulations (Figures 9d and e). Though a one-to-one comparison between M_R and both ρ_s and P through time is not feasible because of the different time resolution of aerial images and numerical simulations, our results advocate that no significant correlations exist between the analyzed parameters (Figures 9d and e). Conversely, a significant, positive correlation (p-value < 0.01) is observed between the relative increase in the average channel cross-sectional area ($\Delta\Omega$, computed from the available bathymetric data) and the relative change in tidal prism (ΔP, calculated through numerical simulations) (Figure 9f). Moreover, comparisons with early data by D'Alpaos et al. (2010) (Figure 9f, inset) confirm that $\{P;\Omega\}$ values from the Gaggian channel are within the range of variability typically emerging from field data.

In view of the above, our results can be straightforwardly interpreted and bear critical implications for tidal-meander geomorphology, as we discuss in the following. First, both direct and induced morphological modifications of the lagoon determined changes in local hydrodynamics within the studied channel, resulting in enhanced local tidal ranges and water discharges (Figures 6a–c). Numerical simulations firmly support this hypothesis, showing that two major increments in local tidal range, flow velocities, and flow discharges occurred: (i) between 1897 and 1901, immediately after the completion of the jetties at the Lido inlet; and (ii) between 1932 and 1970, when the lagoon experienced a significant deepening (Carniello et al., 2009) and loss of salt-marsh areas (Figures 2c and d) as a result of extensive land reclamation and the ongoing exploitation of groundwater resources, which was at its peak during that period. Local modifications of tidal-system properties can lead to far-reaching morphodynamic changes.

Then, increasing water discharges determined adjustments of channel cross-sections through widening and deepening in order to accommodate larger tidal prisms (Figure 9f). In contrast, changes in local tidal asymmetries caused modifications of the local sediment transport regime (Figures 6d–f), resulting in the development of morpho-sedimentary (i.e. bar–pool) patterns according to the dominant tidal phase, as highlighted by bathymetric data (Figure 4) and similar to previous findings regarding both tidal channels in general

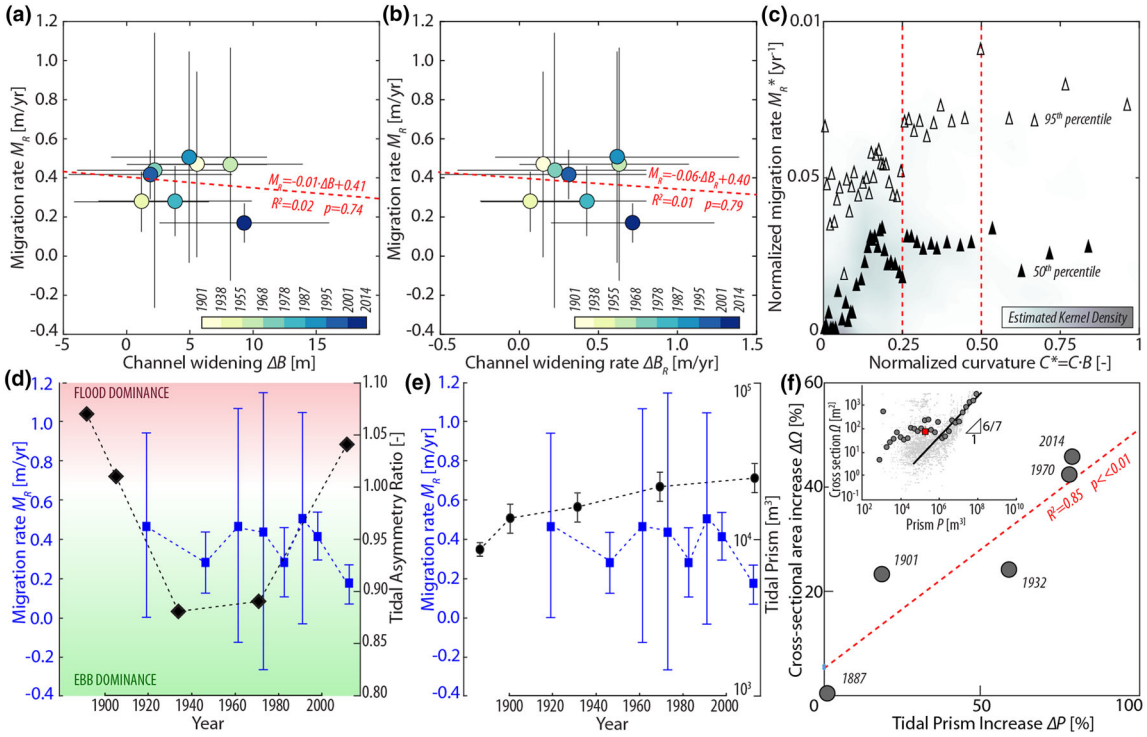

FIGURE 9 Tidal meander morphodynamics. (a, b) Relationships are shown between meander bank migration rates and both changes in channel width (a) and rates thereof (b). (c) Width-normalized migration rates, corrected for the reach-averaged lag between maximum migration and curvature (Sylvester et al., 2019), are plotted against the corresponding width-normalized curvature values. White and black triangles represent the binned 95th and 50th percentiles of the M_R^* distribution, obtained from progressively binning the data into equal sets of 50 points. Shaded areas represent the 2D kernel density estimates of the data. (d, e) Covariance of bank migration rates computed from aerial images and both tidal asymmetry ratio (d) and tidal prism (e) calculated from numerical simulations. (f) Relative changes in channel cross-sectional area as a function of relative tidal prism increase. Dotted red line represents the best linear fit of the data. The inset shows field data from D'Alpaos et al. (2010), with the red point representing average value from the Gaggian channel.

(Tambroni et al., 2017) and the Gaggian channel in particular (Finotello, Canestrelli, et al., 2019). Such bar–pool patterns eventually determine channel migration through a bar-push mechanism (van de Lageweg et al., 2014), whose intensity directly depends on the local channel curvature (Figure 9c) in a fashion similar to river meanders, whereas the direction of migration is dictated by the locally dominant tidal phase (i.e. ebb or flood). Indeed, dynamic time warping of channel centreline migration (Figure 3) highlights changes in the migration direction consistent with the changes in local tidal flow asymmetry. Specifically, progressively larger ebb–peak velocities in the period 1887–1932 led to more pronounced migration on the seaward side of bend apexes, in accordance with earlier field, numerical, and experimental studies (Finotello, Canestrelli, et al., 2019; Tambroni et al., 2017). Such a migration trajectory was maintained, though with reduced magnitude, as tidal flow asymmetry remained nearly constant from 1932 to 1970, whereas a shift to flood-dominated tidal flows, likely dictated by manmade interventions at the Lido inlet and testified by a value of $\rho_s = 1.04$ in 2014, gave rise to inner bank erosion and promoted more symmetric migration, especially around bend apexes (Figure 3).

Different from classic alluvial rivers, however, wherein the highest SSC values are typically observed during the major flood events, we show that SSC is not strictly related to local flow conditions within tidal channels. Rather, high SSC can occur even during slack waters, especially when the growth of wind waves is not impeded by widespread salt-marsh areas that limit wind fetches. Our results indeed suggest that increasingly high SSC values are observed during Bora windstorms (Figure 6f), with markedly more pronounced raises from 1970 onwards, which are most likely dictated by the progressive widening and deepening of tidal flat surfaces at the expense of salt-marsh areas (Carniello et al., 2009; Finotello, Marani, et al., 2020; Tommasini et al., 2019). Such a difference in sediment transport regime has profound implications for the sedimentology of microtidal point-bar deposits, as well as for the development of channel bedforms, as we discuss in the next section.

5.2 | Sedimentology

Aerial photos show that cored point-bar deposits of Bend 1 accreted seaward during the whole study period (Figures 3l–n), which agrees with observational evidence provided by seismic records as highlighted by Ghinassi, Brivio, et al. (2018). Bar accretion arose from the lateral shift of the meander bend driven by secondary currents, transverse to the main flow, which developed from both the curvature of the channel axis (i.e. curvature-driven secondary currents; Figure 9c) and the shoaling effect due to the bar–pool pattern that typically characterizes meandering channels (i.e. topography-driven secondary currents; Figure 4) (Blanckaert & de Vriend, 2004; Camporeale et al., 2007; Johannesson & Parker, 1989). Upbar transport of sediments allows only the finer deposits to reach the bar top, leading to the development of a fining-upward grain-size trend such as that observed in the cored deposits (Figure 8).

Dune-scale bedforms, which only occur locally within the present-day channel, are nearly symmetric in shape and characterized by a low relief and the lack of a defined avalanching front (Figure 7). Our data clearly show that while these bedforms display heights (*H*) and lengths (*L*) similar to those observed in rivers (Bradley & Venditti, 2017), they are characterized by markedly reduced lee-side angles, as well as *H*/*h* ratios, with *h* being the local flow depth (Figure 7). Ratios of *L* to *h* close to 1 (Figure 7d) suggest that dunes in the Gaggian channel are shaped by mechanisms similar to those acting in rivers, though likely mediated by significant amounts of suspended sediment preventing the formation of high-angle dunes (Bradley & Venditti, 2017; Cisneros et al., 2020). Indeed, in the Venice Lagoon, a large amount of mud is suspended from tidal flats by storm waves and flushed into tidal channels, where it can potentially settle down during slack-water periods (Figure 6f). This substantial mobilization of mud, along with the paucity of sandy deposits due to both the lack of any relevant riverine input into the Venice Lagoon (D'Alpaos, 2010; Rinaldo et al., 2008) and sand grain stabilization operated by algal maths (Sfriso et al., 1992, 2001), promotes depositional dynamics potentially similar to that occurring in major rivers characterized by high SSC, where low-angle dunes have been widely documented (Cisneros et al., 2020). The dominance of sediment settling in a nearly symmetric tidal regime could also be responsible for the formation of symmetric bedforms, which were progressively shaped by bidirectional currents with comparable intensities, as testified by the present-day local peak flow asymmetry ($\rho_s = 1.04$).

Integration between sedimentological core data and morphology of surveyed bedforms allows discussion of how tidal processes are documented in the bar deposits. The widespread paucity of cross-stratified deposits fits with the overall lack of high-relief bedforms developed both at the ripple and dune scale, which, on the contrary, are commonly documented in meso- to macrotidal channels (Archer, 2013; Choi, 2011a; Cruz & Noernberg, 2020; Dalrymple et al., 2012; Dalrymple & Choi, 2007; Hughes, 2012). Pervasive laminations conformable to accretion surfaces (Ghinassi, Brivio, et al., 2018) suggest that the bar accreted mainly through progressive draping of its slope, which is also confirmed by the dominance of muddy deposits. The local variability of the dip angle of laminae could fit with the development and preservation of low-angle dunes (Bradley & Venditti, 2017; Cisneros et al., 2020), where suspended sediment bypasses the dune lee and settles in the trough, shaping a more rounded morphology since less sediment is available at the crest to maintain an avalanching front (Hendershot et al., 2016; Kostaschuk et al., 2009). The presence of sporadic ripple cross laminations points to the occurrence of restricted zones where the local availability of sand, possibly due to the reworking of older unconsolidated deposits, allows the development of high-relief bedforms. Therefore, we posit that the mobilization of large volumes of sediment during major storms is responsible for the scarce development of high-relief bedforms, and hinders the accumulation of deposits recording a typical tidal cyclicity, which is commonly well documented where large accretional rates occur (Tessier, 1993). Accordingly, the millimetric intervals showing a progressive change in thickness of laminae (Figure 8) could document parts of neap–spring cycles that occurred during storms lasting 5–6 days, where the larger availability of sediment allowed us to record the progressive change in tidal intensity over a time interval of several days. In this frame, the clearest tidal signature in the studied bar deposits is, therefore, represented by the millimetre-scale mud couples (Figure 8), which are interpreted as double mud drapes (Chen et al., 2015) documenting mud settling during two consecutive slack-water phases. Despite being generated in a purely tidal environment, sedimentary features of the point-bar deposits do not show a clear signature of tidal processes, such as that associated with tidal rhythmites or bundles, providing a warning in interpreting sedimentary successions accumulated in microtidal settings.

Though we claimed that the Gaggian channel represents an ideal proxy for investigating the morphodynamics of microtidal meandering channels, at least in terms of planform morphologies and dynamics, care should be taken when extending the sedimentological results described above to other tidal settings. In particular, sediment dynamics in tidal embayments characterized by limited wind fetches (e.g. where tidal flat areas are reduced compared to salt marshes), more energetic meso- or macrotidal regimes compared to the microtidal setting analysed here (Archer, 2013), and/or different sediment physical properties (e.g. in tidal settings much sandier than the Venice Lagoon) could be much less dependent on the action of wind waves compared to the conditions we illustrated above, thus potentially giving rise to sedimentary features different from those we describe here, especially in term of bedform morphologies and the presence of tidal rhythmites (Bartholdy et al., 2002; Choi, 2010, 2011b; Choi et al., 2013, 2021; Choi & Dalrymple, 2004; Cosma et al., 2022; Dalrymple et al., 2012; Flemming & Bartholoma, 2009; Tessier, 2012; Tessier et al., 1995, 2010). This has potential implications not only for the development of tidal bedforms, but also for the dynamics of meander bends, which are critically influenced by the availability of external sediment supply (Constantine et al., 2014; Horton et al., 2017). However, the paucity of studies on tidal meanders carried out so far prevents a direct and meaningful comparison between the morphodynamics of meander bends found in distinct tidal coastal environments, and calls for new field, numerical, theoretical, and experimental insights into a topic that is of broad interest to the entire community of coastal ecogeomorphologists and managers.

6 | CONCLUSIONS

We have combined historical and present-day multidisciplinary data to reconstruct and interpret the morphodynamic and sedimentological evolution of a meandering channel reach in the microtidal Venice Lagoon (Italy). Blending together remote sensing, field data, and numerical modelling, we demonstrated that natural and anthropogenically induced changes in both external forcings and morphological characteristics of the tidal embayment critically affected the morphodynamic evolution of the channels by changing local hydrodynamics. We observed that changes in local flow rates and peak tidal flow asymmetry produced, respectively, adjustments of the channel cross-sectional area proportional to increasing tidal prism and modifications of the channel-bed morphologies, with depositional bodies forming downstream of the bend apexes relative to the locally dominant tidal flows. Moreover, changes in the channel bar–pool patterns due to variations of tidal flow asymmetries decisively impacted the trajectory of planform evolution of the studied meanders through a bar-push

mechanism, which enhanced secondary flows and promoted channel lateral migration according to the dominant tidal flow in a fluvial-like fashion wherein migration rates depend primarily on local channel curvature. We also demonstrated that modifications of the lagoonal morphologies caused profound alterations to the channel sediment transport regime, directly affecting erosional/depositional dynamics and depositional processes associated with the development of tidal point bars and bedforms. In particular, we argued that wind-driven high concentrations of suspended sediments during slack water conditions can limit the development of high-relief bedforms, as well as the formation and preservation of classic sedimentological signatures of tidal processes in sedimentary deposits associated with meandering channels. The lack of these signatures in a purely tidal environment such as the Venice Lagoon provides a warning in interpreting sedimentary successions accumulated in tidal settings characterized by reduced tidal amplitudes and critically affected by wind-induced sediment transport processes.

ACKNOWLEDGEMENTS

We are grateful for detailed reviews by Zoltan Sylvester and one anonymous reviewer, as well as for steering by the Editor and Associate Editor, which greatly helped to improve the manuscript.

This work was supported by the University of Padova SID2016 project entitled 'From channels to rock record: Morphodynamic evolution of tidal meanders and related sedimentary products' (Grant No. BIRD 168939 to M. Ghinassi) and by the project HYDROSEM (Progetti di Eccellenza CARIPARO 2017, Cassa di Risparmio di Padova e Rovigo): 'Fluvial and tidal meanders of the Venetian-Po plain: From hydrodynamics to stratigraphy' (PI Massimiliano Ghinassi). This scientific activity was also partially performed within the Research Program Venezia 2021, with the contribution of the Provveditorato for the Public Works of Veneto, Trentino Alto Adige and Friuli Venezia Giulia, provided through the concessionary of State Consorzio Venezia Nuova and coordinated by CORILA, Research Line 3.2 (Andrea D'Alpaos [PI]; Massimiliano Ghinassi; Alvise Finotello), as is gratefully acknowledged. Open Access Funding provided by Universita degli Studi di Padova within the CRUI-CARE Agreement.

CONFLICT OF INTEREST

The authors declare that they have no known competing financial interests or personal relationships that could have appeared to influence the work reported in this paper.

DATA AVAILABILITY STATEMENT

All the data are listed in the text, references, and figures. Aerial photos can be freely downloaded upon registration from the University of Venice website (http://mapserver.iuav.it/website/foto_aeree/). Wind and tide data from both the Chioggia anemometer and the CNR oceanographic platform are freely available from the Istituto Superiore per la Protezione e la Ricerca Ambientale (http://www.venezia.isprambiente.it/rete-meteo-mareografica) and the Istituto di Scienze Marine (http://www.ismar.cnr.it/infrastrutture/piattaforma-acqua-alta) websites, respectively. Topographic/hydrographic maps of the Venice Lagoon in its past and present configurations, together with sedimentological data, are accessible from the Atlante della Laguna (http://www.atlantedellalaguna.it/).

ORCID

Alvise Finotello https://orcid.org/0000-0003-2563-8062
Ruggero M. Capperucci https://orcid.org/0000-0001-9089-9715
Andrea D'Alpaos https://orcid.org/0000-0003-1172-8278
Massimiliano Ghinassi https://orcid.org/0000-0003-1696-2071

REFERENCES

Archer, A.W. (2013) World's highest tides: Hypertidal coastal systems in North America, South America and Europe. *Sedimentary Geology*, 284/285, 1–25. Available from: https://doi.org/10.1016/J.SEDGEO.2012.12.007

Bartholdy, J., Bartholoma, A. & Flemming, B.W. (2002) Grain-size control of large compound flow-transverse bedforms in a tidal inlet of the Danish Wadden Sea. *Marine Geology*, 188(3–4), 391–413. Available from: https://doi.org/10.1016/S0025-3227(02)00419-X

Barwis, J.H. (1978) Sedimentology of some South Carolina tidal-creek point bars, and a comparison with their fluvial counterparts. In: Miall, A.D. (Ed.) *Fluvial Sedimentology*. Calgary: Dallas Geological Society, pp. 487–510.

Blanckaert, K. & de Vriend, H.J. (2004) Secondary flow in sharp open-channel bends. *Journal of Fluid Mechanics*, 498, 353–380. Available from: https://doi.org/10.1017/S0022112003006979

Bradley, R.W. & Venditti, J.G. (2017) Reevaluating dune scaling relations. *Earth-Science Reviews*, 165, 356–376. Available from: https://doi.org/10.1016/j.earscirev.2016.11.004

Brivio, L., Ghinassi, M., D'Alpaos, A., Finotello, A., Fontana, A., Roner, M. & Howes, N. (2016) Aggradation and lateral migration shaping geometry of a tidal point bar: An example from salt marshes of the Northern Venice Lagoon (Italy). *Sedimentary Geology*, 343, 141–155. Available from: https://doi.org/10.1016/j.sedgeo.2016.08.005

Camporeale, C., Perona, P., Porporato, A. & Ridolfi, L. (2007) Hierarchy of models for meandering rivers and related morphodynamic processes. *Reviews of Geophysics*, 45, RG1001. Available from: https://doi.org/10.1029/2005RG000185

Carbognin, L., Teatini, P., Tomasin, A. & Tosi, L. (2010) Global change and relative sea level rise at Venice: What impact in term of flooding. *Climate Dynamics*, 35, 1055–1063. Available from: https://doi.org/10.1007/s00382-009-0617-5

Carniello, L., D'Alpaos, A. & Defina, A. (2011) Modeling wind waves and tidal flows in shallow micro-tidal basins. *Estuarine, Coastal and Shelf Science*, 92, 263–276. Available from: https://doi.org/10.1016/j.ecss.2011.01.001

Carniello, L., Defina, A. & D'Alpaos, L. (2009) Morphological evolution of the Venice lagoon: Evidence from the past and trend for the future. *Journal of Geophysical Research: Earth Surface*, 114, 1–10. Available from: https://doi.org/10.1029/2008JF001157

Carniello, L., Defina, A. & D'Alpaos, L. (2012) Modeling sand-mud transport induced by tidal currents and wind waves in shallow microtidal basins: Application to the Venice Lagoon (Italy). *Estuarine, Coastal and Shelf Science*, 102/103, 105–115. Available from: https://doi.org/10.1016/j.ecss.2012.03.016

Carniello, L., Defina, A., Fagherazzi, S. & D'Alpaos, L. (2005) A combined wind wave-tidal model for the Venice lagoon, Italy. *Journal of Geophysical Research: Earth Surface*, 110, 1–15. Available from: https://doi.org/10.1029/2004JF000232

Carniello, L., Silvestri, S., Marani, M., D'Alpaos, A., Volpe, V. & Defina, A. (2014) Sediment dynamics in shallow tidal basins: In situ observations, satellite retrievals, and numerical modeling in the Venice Lagoon. *Journal of Geophysical Research: Earth Surface*, 119, 802–815. Available from: https://doi.org/10.1002/2013JF003015

Chen, S., Steel, R.J. & Olariu, C. (2015) Chapter 7 – Palaeo-Orinoco (Pliocene) channels on the tide-dominated Morne L'Enfer delta lobes and estuaries, SW Trinidad. In: Ashworth, P.J., Best, J.L. & Parsons, D.R. (Eds.) *Developments in Sedimentology*. Amsterdam: Elsevier, pp. 227–281 10.1016/B978-0-444-63529-7.00010-9.

Choi, K., Jo, J. & Kim, D. (2021) Tidal and seasonal controls on the stratigraphic architecture of blind tidal channel deposits in the fluvial–tidal transition of the macrotidal Sittaung River estuary, Myanmar.

Sedimentary Geology, 426, 106029. Available from: https://doi.org/10.1016/j.sedgeo.2021.106029

Choi, K.S. (2010) Rhythmic climbing-ripple cross-lamination in inclined heterolithic stratification (IHS) of a macrotidal estuarine channel, Gomso Bay, west coast of Korea. *Journal of Sedimentary Research*, 80(6), 550–561. Available from: https://doi.org/10.2110/jsr.2010.054

Choi, K.S. (2011a) External controls on the architecture of inclined heterolithic stratification (IHS) of macrotidal Sukmo Channel: Wave versus rainfall. *Marine Geology*, 285(1–4), 17–28. Available from: https://doi.org/10.1016/j.margeo.2011.05.002

Choi, K.S. (2011b) Tidal rhythmites in a mixed-energy, macrotidal estuarine channel, Gomso Bay, west coast of Korea. *Marine Geology*, 280(1–4), 105–115. Available from: https://doi.org/10.1016/j.margeo.2010.12.004

Choi, K.S. & Dalrymple, R.W. (2004) Recurring tide-dominated sedimentation in Kyonggi Bay (west coast of Korea): Similarity of tidal deposits in late Pleistocene and Holocene sequences. *Marine Geology*, 212(1–4), 81–96. Available from: https://doi.org/10.1016/j.margeo.2004.07.008

Choi, K.S., Dalrymple, R.W., Chun, S.S. & Kim, S.P. (2004) Sedimentology of modern, inclined heterolithic stratification (IHS) in the macrotidal Han River Delta, Korea. *Journal of Sedimentary Research*, 74(5), 677–689. Available from: https://doi.org/10.1306/030804740677

Choi, K.S., Hong, C.M., Kim, M.H., Oh, C.R. & Jung, J.H. (2013) Morphologic evolution of macrotidal estuarine channels in Gomso Bay, west coast of Korea: Implications for the architectural development of inclined heterolithic stratification. *Marine Geology*, 346, 343–354. Available from: https://doi.org/10.1016/j.margeo.2013.10.005

Choi, K.S. & Jo, J.H. (2015) Morphodynamics of tidal channels in the open coast macrotidal flat, Southern Ganghwa Island in Gyeonggi Bay, west coast of Korea. *Journal of Sedimentary Research*, 85(6), 582–595. Available from: https://doi.org/10.2110/jsr.2015.44

Cisneros, J., Best, J., van Dijk, T., Almeida, R.P., Amsler, M., Boldt, J. et al. (2020) Dunes in the world's big rivers are characterized by low-angle lee-side slopes and a complex shape. *Nature Geoscience*, 13, 156–162. Available from: https://doi.org/10.1038/s41561-019-0511-7

Coco, G., Zhou, Z., van Maanen, B., Olabarrieta, M., Tinoco, R. & Townend, I.H. (2013) Morphodynamics of tidal networks: Advances and challenges. *Marine Geology*, 346, 1–16. Available from: https://doi.org/10.1016/j.margeo.2013.08.005

Constantine, J.A., Dunne, T., Ahmed, J., Legleiter, C. & Lazarus, E.D. (2014) Sediment supply as a driver of river evolution in the Amazon Basin. *Nature Geoscience*, 7(12), 899–903. Available from: https://doi.org/10.1038/NGEO2282

Cosma, M., Finotello, A., Ielpi, A., Ventra, D., Oms, O., Alpaos, A.D. et al. (2020) Piracy-controlled geometry of tide-dominated point bars: Combined evidence from ancient sedimentary successions and modern channel networks. *Geomorphology*, 370, 107402. Available from: https://doi.org/10.1016/j.geomorph.2020.107402

Cosma, M., Ghinassi, M., D'Alpaos, A., Roner, M., Finotello, A., Tommasini, L. et al. (2019) Point-bar brink and channel thalweg trajectories depicting interaction between vertical and lateral shifts of microtidal channels in the Venice Lagoon (Italy). *Geomorphology*, 342, 37–50. Available from: https://doi.org/10.1016/j.geomorph.2019.06.009

Cosma, M., Lague, D., D'Alpaos, A., Leroux, J., Feldmann, B. & Ghinassi, M. (2022) Sedimentology of a hypertidal point bar (Mont-Saint-Michel Bay, north-western France) revealed by combining lidar time-series and sedimentary core data. *Sedimentology*, 69, 1179–1208. Available from: https://doi.org/10.1111/sed.12942

Cruz, O.G. & Noernberg, A.M. (2020) Bedforms controlled by residual current vortices in a subtropical estuarine tidal channel. *Estuarine, Coastal and Shelf Science*, 232, 106485. Available from: https://doi.org/10.1016/j.ecss.2019.106485

D'Alpaos, A., Carniello, L. & Rinaldo, A. (2013) Statistical mechanics of wind wave-induced erosion in shallow tidal basins: Inferences from the Venice Lagoon. *Geophysical Research Letters*, 40, 3402–3407. Available from: https://doi.org/10.1002/grl.50666

D'Alpaos, A., Finotello, A., Goodwin, G.C.H. & Mudd, S.M. (2021) Salt marsh hydrodynamics. In: FitzGerald, D. & Hughes, Z. (Eds.) *Salt Marshes: Function, Dynamics, and Stresses*. Cambridge: Cambridge University Press, pp. 53–81 10.1017/9781316888933.005.

D'Alpaos, A., Ghinassi, M., Finotello, A., Brivio, L., Bellucci, L.G. & Marani, M. (2017) Tidal meander migration and dynamics: A case study from the Venice Lagoon. *Marine and Petroleum Geology*, 87, 80–90. Available from: https://doi.org/10.1016/j.marpetgeo.2017.04.012

D'Alpaos, A., Lanzoni, S., Marani, M., Fagherazzi, S. & Rinaldo, A. (2005) Tidal network ontogeny: Channel initiation and early development. *Journal of Geophysical Research: Earth Surface*, 110, 1–14. Available from: https://doi.org/10.1029/2004JF000182

D'Alpaos, A., Lanzoni, S., Marani, M. & Rinaldo, A. (2010) On the tidal prism-channel area relations. *Journal of Geophysical Research: Earth Surface*, 115, 1–13. Available from: https://doi.org/10.1029/2008JF001243

D'Alpaos, L. (2010) *Fatti e misfatti di idraulica lagunare. La laguna di Venezia dalla diversione dei fiumi alle nuove opere delle bocche di porto*. Venice: Istituto Veneto di Scienze, Lettere ed Arti.

Dalrymple, R.W., Baker, E.K., Harris, P.T. & Hughes, M.G. (2003) Sedimentology and stratigraphy of a tide-dominated, foreland–basin delta (Fly River, Papua New Guinea). In: Sidi, F.H., Nummedal, D., Imbert, P., Darman, H. & Posamentier, H.W. (Eds.) *Tropical Deltas of Southeast Asia – Sedimentology, Stratigraphy, and Petroleum Geology*. Tulsa, OK: Society for Sedimetary Geology, pp. 147–173 10.2110/pec.03.76.0147.

Dalrymple, R.W. & Choi, K.S. (2007) Morphologic and facies trends through the fluvial–marine transition in tide-dominated depositional systems: A schematic framework for environmental and sequence-stratigraphic interpretation. *Earth-Science Reviews*, 81, 135–174. Available from: https://doi.org/10.1016/j.earscirev.2006.10.002

Dalrymple, R.W., Mackay, D.A., Ichaso, A.A. & Choi, K.S. (2012) Processes, morphodynamics, and facies of tide-dominated estuaries. In: Davis, R.A., Jr. & Dalrymple, R.W. (Eds.) *Principles of Tidal Sedimentology*. Dordrecht: Springer Science+Business Media, pp. 79–107.

de Mowbray, T. (1983) The genesis of lateral accretion deposits in recent intertidal mudflat channels, Solway Firth, Scotland. *Sedimentology*, 30(3), 425–435. Available from: https://doi.org/10.1111/j.1365-3091.1983.tb00681.x

Defina, A. (2000) Two-dimensional shallow flow equations for partially dry areas. *Water Resources Research*, 36(11), 3251–3264. Available from: https://doi.org/10.1029/2000WR900167

Donovan, M., Belmont, P. & Sylvester, Z. (2021) Evaluating the relationship between meander-bend curvature, sediment supply, and migration rates. *Journal of Geophysical Research: Earth Surface*, 126, 1–20. Available from: https://doi.org/10.1029/2020JF006058

Fenies, H. & Faugères, J.C. (1998) Facies and geometry of tidal channel-fill deposits (Arcachon Lagoon, SW France). *Marine Geology*, 150(1–4), 131–148. Available from: https://doi.org/10.1016/S0025-3227(98)00049-8

Feola, A., Belluco, E., D'Alpaos, A., Lanzoni, S., Marani, M. & Rinaldo, A. (2005) A geomorphic study of lagoonal landforms. *Water Resources Research*, 41, 1–11. Available from: https://doi.org/10.1029/2004WR003811

Ferrarin, C., Tomasin, A., Bajo, M., Petrizzo, A. & Umgiesser, G. (2015) Tidal changes in a heavily modified coastal wetland. *Continental Shelf Research*, 101, 22–33. Available from: https://doi.org/10.1016/j.csr.2015.04.002

Finotello, A., Canestrelli, A., Carniello, L., Ghinassi, M. & D'Alpaos, A. (2019) Tidal flow asymmetry and discharge of lateral tributaries drive the evolution of a microtidal meander in the Venice Lagoon (Italy). *Journal of Geophysical Research: Earth Surface*, 124, 3043–3066. Available from: https://doi.org/10.1029/2019jf005193

Finotello, A., D'Alpaos, A., Bogoni, M., Ghinassi, M. & Lanzoni, S. (2020) Remotely-sensed planform morphologies reveal fluvial and tidal nature of meandering channels. *Scientific Reports*, 10(54), 1–13. Available from: https://doi.org/10.1038/s41598-019-56992-w

Finotello, A., D'Alpaos, A., Lazarus, E.D. & Lanzoni, S. (2019) High curvatures drive river meandering – Comment. *Geology*, 47, e485. Available from: https://doi.org/10.1130/G46761C.1

Finotello, A., Ghinassi, M., Carniello, L., Belluco, E., Pivato, M., Tommasini, L. & D'Alpaos, A. (2020) Three-dimensional flow structures and morphodynamic evolution of microtidal meandering channels. *Water Resources Research*, 56(7), e2020WR027822. Available from: https://doi.org/10.1029/2020WR027822

Finotello, A., Lanzoni, S., Ghinassi, M., Marani, M., Rinaldo, A. & D'Alpaos, A. (2018) Field migration rates of tidal meanders recapitulate fluvial morphodynamics. *Proceedings of the National Academy of Sciences of the United States of America*, 115(7), 1463–1468. Available from: https://doi.org/10.1073/pnas.1711330115

Finotello, A., Marani, M., Carniello, L., Pivato, M., Roner, M., Tommasini, L. & D'Alpaos, A. (2020) Control of wind-wave power on morphological shape of salt marsh margins. *Water Science and Engineering*, 13(1), 45–56. Available from: https://doi.org/10.1016/j.wse.2020.03.006

Flemming, B.W. (1988) Zur Klassifikation subaquatischer, strömungstransversaler Transportkörper; 93–97.

Flemming, B.W. & Bartholoma, A. (2009) *Tidal Signatures in Modern and Ancient Sediments*. New York: Wiley Interscience.

Friedrichs, C.T. & Aubrey, D.G. (1988) Nonlinear tidal distortion in shallow well-mixed estuaries. *Estuarine, Coastal and Shelf Science*, 27, 521–545. Available from: https://doi.org/10.1016/0272-7714(90)90054-U

Gabet, E.J. (1998) Lateral migration and bank erosion in a saltmarsh tidal channel in San Francisco Bay, California. *Estuaries*, 21(4), 745–753. Available from: https://doi.org/10.2307/1353278

Garofalo, D. (1980) The influence of wetland vegetation on tidal stream channel migration and morphology. *Estuaries*, 3(4), 258–270. Available from: https://doi.org/10.2307/1352081

Gatto, P. & Carbognin, L. (1981) The Lagoon of Venice: natural environmental trend and man-induced modification / La Lagune de Venise: l'évolution naturelle et les modifications humaines. *Hydrological Sciences Bulletin*, 26(4), 379–391. Available from: https://doi.org/10.1080/02626668109490902

Ghezzo, M., Guerzoni, S., Cucco, A. & Umgiesser, G. (2010) Changes in Venice Lagoon dynamics due to construction of mobile barriers. *Coastal Engineering*, 57, 694–708. Available from: https://doi.org/10.1016/j.coastaleng.2010.02.009

Ghinassi, M., Brivio, L., D'Alpaos, A., Finotello, A., Carniello, L., Marani, M. & Cantelli, A. (2018) Morphodynamic evolution and sedimentology of a microtidal meander bend of the Venice Lagoon (Italy). *Marine and Petroleum Geology*, 96, 391–404. Available from: https://doi.org/10.1016/j.marpetgeo.2018.06.011

Ghinassi, M., D'Alpaos, A., Tommasini, L., Brivio, L., Finotello, A. & Stefani, C. (2019) Tidal currents and wind waves controlling sediment distribution in a subtidal point bar of the Venice Lagoon (Italy). *Sedimentology*, 66(7), 2926–2949. Available from: https://doi.org/10.1111/sed.12616

Ghinassi, M., D'Alpaos, A., Gasparotto, A., Carniello, L., Brivio, L., Finotello, A. et al. (2018) Morphodynamic evolution and stratal architecture of translating tidal point bars: Inferences from the northern Venice Lagoon (Italy). *Sedimentology*, 65(4), 1354–1377. Available from: https://doi.org/10.1111/sed.12425

Giorgino, T. (2009) Computing and visualizing dynamic time warping alignments in R: The dtw package. *Journal of Statistical Software*, 31(7), 1–24. Available from: https://doi.org/10.18637/jss.v031.i07

Guo, L., Wang, Z.B., Townend, I. & He, Q. (2019) Quantification of tidal asymmetry and its nonstationary variations. *Journal of Geophysical Research: Oceans*, 124, 773–787. Available from: https://doi.org/10.1029/2018JC014372

Hendershot, M.L., Venditti, J.G., Bradley, R.W., Kostaschuk, R.A., Church, M. & Allison, M.A. (2016) Response of low-angle dunes to variable flow. *Sedimentology*, 63, 743–760. Available from: https://doi.org/10.1111/sed.12236

Hickin, E.J. & Nanson, G.C. (1975) The character of channel migration on the Beatton River, northeast British Columbia, Canada. *Bulletin of the Geological Society of America*, 86, 487–494. Available from: https://doi.org/10.1130/0016-7606(1975)86<487:TCOCMO>2.0.CO;2

Hooke, J.M. (2013) River meandering. In: Wohl, E. & Schroder, J. (Eds.) *Treatise on Geomorphology*. San Diego, CA: Academic Press, pp. 260–288.

Horton, A.J., Constantine, J.A., Hales, T.C., Goossens, B., Bruford, M.W. & Lazarus, E.D. (2017) Modification of the mechanisms driving river meandering caused by tropical deforestation. *Geology*, 46, 511–514. Available from: https://doi.org/10.1130/G38740.1

Hughes, Z.J. (2012) Tidal channels on tidal flats and marshes. In: Davis, R. A. & Dalrymple, R.W. (Eds.) *Principles of Tidal Sedimentology*. Dordrecht: Springer, pp. 269–300.

Ielpi, A., Lapôtre, M.G.A., Finotello, A., Ghinassi, M. & D'Alpaos, A. (2020) Channel mobility drives a diverse stratigraphic architecture in the dryland Mojave River (California, USA). *Earth Surface Processes and Landforms*, 45(8), 1717–1731. Available from: https://doi.org/10.1002/esp.4841

Ikeda, S., Parker, G. & Sawai, K. (1981) Bend theory of river meanders. Part 1. Linear development. *Journal of Fluid Mechanics*, 112, 363–377. Available from: https://doi.org/10.1017/S0022112081000451

Johannesson, H. & Parker, G. (1989) Secondary flow in mildy sinuous channel. *Journal of Hydraulic Research*, 115, 289–308. Available from: https://doi.org/10.1061/(ASCE)0733-9429(1989)115:3(289)

Kästner, K., Hoitink, A.J.F., Vermeulen, B., Geertsema, T.J. & Ningsih, N.S. (2017) Distributary channels in the fluvial to tidal transition zone. *Journal of Geophysical Research: Earth Surface*, 122(3), 696–710. Available from: https://doi.org/10.1002/2016JF004075

Kleinhans, M.G., Schuurman, F., Bakx, W. & Markies, H. (2009) Meandering channel dynamics in highly cohesive sediment on an intertidal mud flat in the Westerschelde estuary, the Netherlands. *Geomorphology*, 105(3–4), 261–276. Available from: https://doi.org/10.1016/j.geomorph.2008.10.005

Kostaschuk, R., Shugar, D., Best, J., Parsons, D.R., Lane, S., Hardy, R. & Orfeo, O. (2009) Suspended sediment transport and deposition over a dune: Río Paraná, Argentina. *Earth Surface Processes and Landforms*, 34(12), 1605–1611. Available from: https://doi.org/10.1002/esp.1847

Lanzoni, S. & Seminara, G. (2006) On the nature of meander instability. *Journal of Geophysical Research: Earth Surface*, 111(F4), F4F04006. Available from: https://doi.org/10.1029/2005JF000416

Lefebvre, A. & Winter, C. (2016) Predicting bed form roughness: The influence of lee side angle. *Geo-Marine Letters*, 36(2), 121–133. Available from: https://doi.org/10.1007/s00367-016-0436-8

Leuven, J.R.F.W., van Maanaen, B., Lexmond, B.R., van der Hoek, B.V., Spruijt, M.J. & Kleinhans, M.G. (2018) Dimensions of fluvial–tidal meanders: Are they disproportionally large? *Geology*, 46(10), 923–926. Available from: https://doi.org/10.1130/G45144.1/4332136/g45144.pdf

Madricardo, F., Foglini, F., Kruss, A., Ferrarin, C., Pizzeghello, N.M., Murri, C. et al. (2017) High resolution multibeam and hydrodynamic datasets of tidal channels and inlets of the Venice Lagoon. *Scientific Data*, 4(1), 170121. Available from: https://doi.org/10.1038/sdata.2017.121

Marani, M., Belluco, E., D'Alpaos, A., Defina, A., Lanzoni, S., Rinaldo, A. et al. (2003) On the drainage density of tidal networks. *Water Resources Research*, 39(2), 1–11. Available from: https://doi.org/10.1029/2001WR001051

Matticchio, B., Carniello, L., Canesso, D., Ziggiotto, E., Cordella, M. (2017) Recent changes in tidal propagation in the Venice Lagoon: Effects of changes in the inlet structure. In: D'Alpaos, L. (Ed.) *Commissione di studio sui problemi di Venezia, Volume III: La laguna di Venezia e le nuove opere alle bocche*. Venice, Italy: Istituto Veneto di Scienze, Lettere ed Arti, pp. 157–183. (ISBN ebook: 978-88-95996-77-6. [in italian]).

McClennen, C.E. & Housley, R.A. (2006) Late-Holocene channel meander migration and mudflat accumulation rates, Lagoon of Venice, Italy. *Journal of Coastal Research*, 22, 930–945. Available from: https://doi.org/10.2112/03-0113.1

McMahon, W.J. & Davies, N.S. (2019) The shortage of geological evidence for pre-vegetation meandering rivers. In: Ghinassi, M., Colombera, L., Mountney, N.P., Reesink, A.J. & Bateman, M. (Eds.) *Fluvial Meanders and Their Sedimentary Products in the Rock Record*. Chichester: Wiley, pp. 119–148.

Mel, R., Carniello, L. & D'Alpaos, L. (2019) Addressing the effect of the Mo.S.E. barriers closure on wind setup within the Venice Lagoon. *Estuarine, Coastal and Shelf Science*, 225, 106249. Available from: https://doi.org/10.1016/j.ecss.2019.106249

Mel, R. & Lionello, P. (2014) Verification of an ensemble prediction system for storm surge forecast in the Adriatic Sea. *Ocean Dynamics*, 64(12), 1803–1814. Available from: https://doi.org/10.1007/s10236-014-0782-x

Parker, G., Sawai, K. & Ikeda, S. (1982) Bend theory of river meanders. Part 2. Nonlinear deformation of finite-amplitude bends. *Journal of Fluid Mechanics*, 115(1), 303–314. Available from: https://doi.org/10.1017/S0022112082000767

Rinaldo, A., Nicótina, L., Alessi Celegon, E., Beraldin, F., Botter, G., Carniello, L. et al. (2008) Sea level rise, hydrologic runoff, and the flooding of Venice. *Water Resources Research*, 44(12), 1–12. Available from: https://doi.org/10.1029/2008WR007195

Sarretta, A., Pillon, S., Molinaroli, E., Guerzoni, S. & Fontolan, G. (2010) Sediment budget in the Lagoon of Venice, Italy. *Continental Shelf Research*, 30(8), 934–949. Available from: https://doi.org/10.1016/j.csr.2009.07.002

Seminara, G. (2006) Meanders. *Journal of Fluid Mechanics*, 554(1), 271–297. Available from: https://doi.org/10.1017/S0022112006008925

Sfriso, A., Birkemeyer, T. & Ghetti, P.F. (2001) Benthic macrofauna changes in areas of Venice Lagoon populated by seagrasses or seaweeds. *Marine Environmental Research*, 52(4), 323–349. Available from: https://doi.org/10.1016/S0141-1136(01)00089-7

Sfriso, A., Pavoni, B., Marcomini, A. & Orio, A.A. (1992) Macroalgae, nutrient cycles, and pollutants in the Lagoon of Venice. *Estuaries*, 15(4), 517–528. Available from: https://doi.org/10.2307/1352394

Silvestri, S., D'Alpaos, A., Nordio, G. & Carniello, L. (2018) Anthropogenic modifications can significantly influence the local mean sea level and affect the survival of salt marshes in shallow tidal systems. *Journal of Geophysical Research: Earth Surface*, 123(5), 996–1012. Available from: https://doi.org/10.1029/2017JF004503

Solari, L., Seminara, G., Lanzoni, S., Marani, M. & Rinaldo, A. (2002) Sand bars in tidal channels. Part 2. Tidal meanders. *Journal of Fluid Mechanics*, 451, 203–238. Available from: https://doi.org/10.1017/S0022112001006565

Soulsby, R.L. (1997) *Dynamics of Marine Sands: A Manual for Practical Applications*. London: Thomas Telford.

Sylvester, Z., Durkin, P. & Covault, J.A. (2019) High curvatures drive river meandering. *Geology*, 47(3), 263–266. Available from: https://doi.org/10.1130/G46838Y.1

Tambroni, N., Luchi, R. & Seminara, G. (2017) Can tide dominance be inferred from the point bar pattern of tidal meandering channels? *Journal of Geophysical Research: Earth Surface*, 122(2), 1–21. Available from: https://doi.org/10.1002/2016JF004139

Tessier, B. (1993) Upper intertidal rhythmites in the Mont-Saint-Michel Bay (NW France): Perspectives for paleoreconstruction. *Marine Geology*, 110(3–4), 355–367. Available from: https://doi.org/10.1016/0025-3227(93)90093-B

Tessier, B. (2012) Stratigraphy of tide-dominated estuaries. In: Davis, R. A. & Dalrymple, R.W. (Eds.) *Principles of Tidal Sedimentology*. Cham: Springer Nature, pp. 109–128 10.1007/978-94-007-0123-6_6.

Tessier, B., Archer, A.W., Lanier, W.P. & Feldman, H.R. (1995) Comparison of ancient tidal rhythmites (carboniferous of Kansas and Indiana, USA) with modern analogues (the Bay of Mont-Saint-Michel, France). In: Flemming, B.W. & Bartholoma, A. (Eds.) *Tidal Signatures in Modern and Ancient Sediments*. Chichester: Wiley, pp. 259–271 10.1002/9781444304138.ch17.

Tessier, B., Billeaud, I. & Lesueur, P. (2010) Stratigraphic organisation of a composite macrotidal wedge: The Holocene sedimentary infilling of the Mont-Saint-Michel Bay (NW France). *Bulletin de la Societe Geologique de France*, 181(2), 99–113. Available from: https://doi.org/10.2113/gssgfbull.181.2.99

Tomasin, A. (1974) Recent changes in the tidal regime in Venice. *Rivista Italiana di Geofisica*, 23, 275–278.

Tommasini, L., Carniello, L., Ghinassi, M., Roner, M. & D'Alpaos, A. (2019) Changes in the wind-wave field and related salt-marsh lateral erosion: Inferences from the evolution of the Venice Lagoon in the last four centuries. *Earth Surface Processes and Landforms*, 44(8), 1633–1646. Available from: https://doi.org/10.1002/esp.4599

Townend, I.H. (2010) An exploration of equilibrium in Venice Lagoon using an idealised form model. *Continental Shelf Research*, 30(8), 984–999. Available from: https://doi.org/10.1016/j.csr.2009.10.012

Valle-Levinson, A., Marani, M., Carniello, L., D'Alpaos, A. & Lanzoni, S. (2021) Astronomic link to anomalously high mean sea level in the northern Adriatic Sea. *Estuarine, Coastal and Shelf Science*, 257, 107418. Available from: https://doi.org/10.1016/j.ecss.2021.107418

van de Lageweg, W.I., van Dijk, W.M., Baar, A.W., Rutten, J. & Kleinhans, M.G. (2014) Bank pull or bar push: What drives scroll-bar formation in meandering rivers? *Geology*, 42, 319–322. Available from: https://doi.org/10.1130/G35192.1

Wang, C., Menenti, M., Stoll, M., Feola, A., Belluco, E. & Marani, M. (2009) Separation of ground and low vegetation signatures in LiDAR measurements of salt-marsh environments. *IEEE Transactions on Geoscience and Remote Sensing*, 47, 2014–2023. Available from: https://doi.org/10.1109/TGRS.2008.2010490

Wilson, C., Goodbred, S., Small, C., Gilligan, J., Sams, S., Mallick, B. et al. (2017) Widespread infilling of tidal channels and navigable waterways in the human-modified tidal deltaplain of southwest Bangladesh. *Elementa*, 5(78), 1–12. Available from: https://doi.org/10.1525/elementa.263

Zecchin, M., Baradello, L., Brancolini, G., Donda, F., Rizzetto, F. & Tosi, L. (2008) Sequence stratigraphy based on high-resolution seismic profiles in the late Pleistocene and Holocene deposits of the Venice area. *Marine Geology*, 253(3–4), 185–198. Available from: https://doi.org/10.1016/j.margeo.2008.05.010

How to cite this article: Finotello, A., Capperucci, R.M., Bartholomä, A., D'Alpaos, A. & Ghinassi, M. (2022) Morpho-sedimentary evolution of a microtidal meandering channel driven by 130 years of natural and anthropogenic modifications of the Venice Lagoon (Italy). *Earth Surface Processes and Landforms*, 1–17. Available from: https://doi.org/10.1002/esp.5396